NUREG/CR-1403
BNL-NUREG-51178

WATER REACTOR SAFETY RESEARCH DIVISION

QUARTERLY PROGRESS REPORT
OCTOBER 1 - DECEMBER 31, 1979

Date Published - April 1980

DEPARTMENT OF NUCLEAR ENERGY, BROOKHAVEN NATIONAL LABORATORY
UPTON, NEW YORK 11973

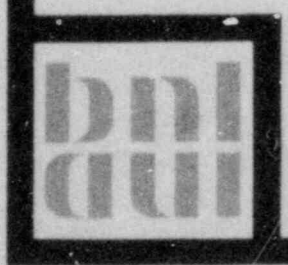

Prepared for the U.S. Nuclear Regulatory Commission
Office of Nuclear Regulatory Research
Contract No. DE-AC02-76CH00016

NUREG/CR-1403
BNL-NUREG-51178
AN, R-1,4,5

WATER REACTOR SAFETY RESEARCH DIVISION

QUARTERLY PROGRESS REPORT
OCTOBER 1 - DECEMBER 31, 1979

HERBERT J.C. KOUTS, Department Chairman
WALTER Y. KATO, Associate Chairman for Reactor Safety

Principal Investigators:

D.J. Diamond
O.C. Jones, Jr.
M.M. Levine
W.G. Shier, Jr.
D. van Rooyen

Compiled by Anthony J. Romano
Manuscript Completed: March 1980

DEPARTMENT OF NUCLEAR ENERGY
BROOKHAVEN NATIONAL LABORATORY, ASSOCIATED UNIVERSITIES, INC.
UPTON, NEW YORK 11973

Prepared for the
REACTOR SAFETY RESEARCH DIVISION
OFFICE OF NUCLEAR REGULATORY RESEARCH
U.S. NUCLEAR REGULATORY COMMISSION
CONTRACT NO. DE-AC02-76CH00016
FIN Nos.:
A-3014 A-3045
A-3208

Available from
GPO Sales Program
Division of Technical Information and Document Control
U.S. Nuclear Regulatory Commission
Washington, D.C. 20555
and
National Technical Information Service
Springfield, Virginia 22161

FOREWORD

The Water Reactor Safety Research Programs Quarterly Report describes current activities and technical progress in the programs at Brookhaven National Laboratory sponsored by the USNRC Division of Reactor Safety Research. The projects reported each quarter are the following: LWR Thermal Hydraulic Development, Advanced Code Evaluation, RELAP Code Assessment, and Stress Corrosion Cracking of PWR Steam Generator Tubing.

The previous reports, BNL-NUREG-50624, BNL-NUREG-50661, BNL-NUREG-50683, BNL-NUREG-50747, BNL-NUREG-50785, BNL-NUREG-50820, BNL-NUREG-50883, BNL-NUREG-50931, BNL-NUREG-50978, BNL-NUREG-51015, BNL-NUREG-51081, and BNL-NUREG-51131 have covered the periods October 1, 1976 through September 30, 1979.

WATER REACTOR SAFETY RESEARCH

TABLE OF CONTENTS

I. LIGHT WATER REACTOR SAFETY

Summary

In the modeling developed to calulate the nonequilibrium vapor generation rates, the nucleation inception and the bubble growth have been treated separately. Fixing the flashing onset by means of the Alamgir-Lienhard correlation at the nozzle throat for BNL experiments provides a method to determine the degree of superheat (pressure) at the inception point and to calculate the critical radius of the bubbles formed. Assuming nucleation to take place only on the pipe walls, the only free parameter left was the packing density of the bubbles on the wall at the inception point. A value chosen for this parameter in turn fixes α_o and C_T for the specific conditions. With the above determined conditions the vapor generation equation was solved and the void profiles calculated. The results were compared with the experimental area averaged void fractions obtained in the last series of runs.

The range of C_T's obtained for the BNL experiments compares favorably with the values of C_T found in pipe flows at lower mass fluxes by Reocreux (1974). The void predictions diverged from the experimental data for $\alpha>0.25$ which is associated with the transition from bubbly to slug flows. This indicates that as expected the conduction-limited bubble growth model is applicable only to bubly flows.

The experimental data of five runs were also compared to TRAC-P1A predictions.

The BNL jet pump-recirculation loop model which was recently added to the code is being modified so that the jet pump M ratio can be specified as an input number. A new fuel rod model was implemented and improves agreement with available data. Nineteen trips have been implemented into the code. Code assessment continues with comparisons being made against measured data and data from another code. Specific problems related to using the code were investigated.

Work on the independent TRAC-P1A assessment has continued with the Moby-Dick nitrogen-water experiments, Marviken critical flow tests, RPI phase separation tests and the FRIGG loop tests. The TRAC-predictions of the Moby-Dick nitrogen-water tests showed significant sensitivity to the two-phase friction factor options. However, the predictions for the Marviken tests were not that sensitive to this option. In spite of many attempts, no converged steady-state TRAC-prediction was obtained for either the RPI phase separation tests (without rods) or the FRIGG-loop tests (with rods and heating).

The spatial plotting capability of the associated plotting code, TRGRIT, was expanded. Also, a BNL version of the TRAC-P1A/MOD1 with more accurate surface tension calculation was made available.

1. Nonequilibrium Phase Change Studies (O.C. Jones, Jr.)

1.1 Purpose of Project

The major purpose of this project is to develop improved analytical descriptions of nonequilibrium liquid-vapor phase change processes for use in advanced computer codes with particular reference to the post dryout regime and to the decompressive flashing regime. Experimental data were to be obtained to provide baseline information where insufficient data existed. In addition, both local and global instrumentation developments were to be undertaken to provide support as necessary to the overall effort.

To accomplish these goals, the following three tasks have been identified:

I. Analytical Modeling;

II. Flashing Experiments;

III. Instrumentation Development;

It is the purpose of this report to briefly summarize the status of each task, the work accomplished previous to the reporting period, and the specific project accomplishments during this quarter.

1.2 Summary of Previous Progress

1.2.1. Task I. Analytical Modeling

In the model developed to calculate the nonequilibrium vapor generation rates, it was decided to treat the nucleation inception point and the bubble growth separately. The nucleation inception point is usually under varying degrees of nonequilibrium and constitutes the origin of the time scale for the bubble growth history.

For flowing systems in pipes and in nozzles, the inception points were related to the Alamgir and Lienhard's (1979) static onset correlation. For the bubbly flow regime ($0 < \alpha < 0.25$), a conduction dominated bubble growth model was proposed by Saha (1977) and Wu (1979). The above mentioned model was applied to the experimental data of Reocreux (1974) and the values of the three unknown parameters, inception point, Z_{NVG}, initial void fraction, α_o, and the parameter C_Γ were determined by the "best fit" to the void data. In reality Z_{NVG}, α_o and C_Γ are all related to each other once the inception point is determined, and such a method was pursued during this quarter and was applied to the BNL flashing experiments.

1.2.2 Task II. Flashing Experiments.

Previous to the reporting quarter, three series of flashing experiments had been completed and reported (Zimmer 1979). A fourth series of flashing experiments was initiated to fulfill the proposed test matrix. Two groups of runs were executed at inlet temperatures of 100 and 120C at various inlet mass fluxes and pressure distributions were measured as well as area averaged void profiles. There are still fifteen experiments to be performed to complete the test matrix,

as well as some repeats if necessary

1.3 Accomplishments During Reporting Period.

1.3.1 Task I. Analytical Modeling (B.J.C. Wu, N. Abuaf)

Calculation of Vapor Generation Rates and Comparison with Experiments.

Flashing as a result of rapid depressurization of liquid flows in commercial pipes is most likely initiated by heterogeneous nucleation of vapor bubbles in the bulk liquid and/or at crevices or microcavities along the wall with pre-existing gas phase. Following Oswatitsch's (1942) treatment of condensation in supersonic nozzles, Zuber, et al. (1966) proposed an expression for the calculation of the mass flow rate of vapor G_g over a cross section located at a point Z along a duct of constant cross section A_c:

$$G_g(Z) = \frac{1}{A_c} \int_{Z_o}^{Z} \xi_h \, m\,(Z, \zeta)\, J(\zeta)\, d\zeta$$

where ξ_h is the perimeter of the duct, $J(\zeta)$ is the nucleation rate per unit wall area at point ζ along the pipe, $m(Z,\zeta)$ is the mass at Z of a vapor bubble nucleated at ζ and Z_o is a point upstream of the nucleation zone. The integration effectively sums the vapor mass of all the bubbles nucleated before the point Z. Although Oswatitsch's model has been applied to the study of condensation in high speed flows (Wegener and Wu 1977) with remarkable success, its extension to flashing flow or subcooled boiling has been difficult. This is mainly because our lack of understanding of the heterogeneous nucleation process.

To circumvent this difficulty, it was decided to treat the nucleation and bubble growth separately. The nucleation onset point which is usually under varying degrees of nonequilibrium conditions strongly affects the subsequent vapor generation rate calculations through several factors. The thermodynamic conditions at this inception point determines the local inception superheat, i.e., the local pressure and thus the critical bubble radius at onset. The same inception point also constitutes the origin of the time scale for the bubble growth history, and thus forms the starting point for all the void development integration schemes and also fixes the initial superheat or driving force for the vapor generation and void growth. The correlation developed by Alamgir-Lienhard (1979) relating the static pressure undershoot below the saturation pressure (at inlet temperature) at the inception point to the reduced initial temperature and local depressurization rate was extended both to pipe flows (Jones 1979) and nozzle flows to determine the flashing inception point.

Next, the local vapor generation rate in the bubble growth region may be calculated from conduction limited bubble growth equations developed by Jones and Zuber (1978) but locally approximated by those first derived by Forster and Zuber (1954) and Plesset and Zwick (1954). The local vapor generation rate depends primarily on three quantities which are unknown a priori:

a. The onset of flashing or inception point, Z_{NVG}, which is usually

under nonequilibrium conditions and constitutes the origin of the time scale for the bubble growth history;

b. The initial void fraction α_o, at the point of inception; and

c. A quantity C_Γ, which is related to the number of bubbles generated at the inception point.

This above-mentioned conduction controlled vapor generation rate was applied to the experimental data of Reocreux (1974), and the values of these three parameters, Z_{NVG}, α_o, and C_Γ were determined by the "best fit" to the void data (Wu 1979). In reality, they are all related to each other. If the inception superheat is specified, thereby determining the onset location Z_{NVG}, the critical bubble radius at the onset of nucleation is also known. Assuming all vapor bubbles are of critical size at inception point, the value of the initial void fraction, α_o, is then uniquely related to the bubble population at the inception point.

The approach followed consisted in solving and integrating the vapor generation equation (Eq. 7, Wu, 1979) by independently determining the unknown parameters. The onset of flashing or inception point Z_{NVG}, was fixed from a semi-empirical onset correlation. The Alamgir-Lienhard (1979) correlation relating the pressure undershoot below P_{sat} at the inception point to the reduced initial temperature and depressurization rate was used.* Once the inception point pressure was determined, the critical radius at the onset point was calculated and assuming nucleation to take place only on the pipe walls, the only free parameter left was the packing density of bubbles on the wall at inception point. A value chosen for this free parameter in turn fixed α_o and C_Γ for the specific conditions. With the above determined values of the parameters Z_{NVG}, α_o and C_Γ, the vapor generation equation (Eq. 7, Wu 1979) was solved and its solution provided the full details of the nonequilibrium transitional region where vapor generation took place.

Since flashing inception in converging-diverging nozzle flows with subcooled inlet conditions always occurred at or near the throat, Z_{NVG} was fixed at the throat location (Abuaf, 1979). Thus, for the BNL experiments,

$$Z_{NVG} = 304.8 \text{ mm} \tag{1.1}$$

Assuming in addition the vapor bubbles at the inception point were all spheres of equal size which was equal to the critical bubble radius r_{crit} corresponding to the local thermodynamic state, it was possible to relate α_o to C_Γ based on purely geometrical considerations:

$$\alpha_o = 0.0532 \, (C_\Gamma \, r_{crit})^3 \, . \tag{1.2}$$

The numerical factor arose from the spherical geometry of the voids. Next, the

* This definition may be refined by coupling with the turbulence correlation of Jones (1979) to determine the onset point or Z_{NVG}. Actually, the latter has been heretofore considered unimportant in nozzles where boundary layer effects are suppressed, and the static inception correlation was directly applied to the nozzle flows.

ideas of Alamgir and Lienhard (1979) were extended to steady flows in a nozzle, where depressurization occurred as a result of convective motion of the fluid. There were some minor conceptual difficulties in transforming Alamgir and Lienhard's Lagrangian treatment to an Eulerian description suitable for application to nozzle flows, since the bubbles were generated at nucleation sites on solid surfaces which did not move with the fluid. In contrast, if the nucleation sites were distributed volumetrically in the fluid, strict correspondence between nucleation processes in steady and unsteady flows could be found. (See, e.g. the treatment of unsteady condensation problems by Wu, 1977 and that of steady flow by Wegener and Wu 1977.) However, in view of the more serious uncertainty associated with the number of available nucleation sites, these minor difficulties were not pursued further. Thus, following Alamgir and Lienhard, it was assumed that at flashing inception a certain fraction of the wall was covered with vapor bubbles of critical size. The cross-sectional averaged values of bubble number density N, and α_o were functions of the local wall geometry. Thus

$$N = \frac{1}{\eta} \frac{1}{\sqrt{3}\, r_{crit}^2\, R} = \frac{1}{1.732\eta\, r_{crit}^2\, R} , \tag{1.3}$$

and

$$\alpha_o = \frac{1}{\eta} \frac{4\pi}{3\sqrt{3}} \frac{r_{crit}}{R} = \frac{2.418}{\eta} \frac{r_{crit}}{R} , \tag{1.4}$$

where R was the local radius of the test section and η was a measure of the bubble packing density. If the wall was completely covered with bubbles, $\eta = 1$; if only 1% of the wall was covered, $\eta = 100$; etc. The corresponding C_Γ was

$$C_\Gamma = 3.569\, (\eta\, r_{crit}^2\, R)^{-1/3} \tag{1.5}$$

Thus, with Z_{NVG} fixed at the throat location, only η was unknown. The value of η was found by comparison of this model with the experimental results. In the current work, η was found by iteration: a value of η was assumed, the corresponding α_o and C_Γ calculated and the integration outlined by Wu (1979) was carried out. The procedure was repeated for a new η until agreement was reached between the calculated and measured area-averaged α-distributions.

To account for the change in flow kinetic energy as a result of area variation in the nozzle, the local specific enthalpy of the flow was estimated from adiabatic flow with zero slip:

$$h_m + \frac{1}{2} \frac{G^2}{\rho_m^2} = \text{const} = h_o \tag{1.6}$$

where h_o was the stagnation enthalpy. The local mass flux of the mixture was given by the continuity equation

$$G/G_{in} = A_{in}/A , \tag{1.7}$$

where the effective area ratio obtained from hydrodynamic calibration of the test section, rather than the geometric value, was used to account for frictional effects in an approximate manner.

In a few of the last series of experiments, Exp. 116-148, larger fluctuations in p_{in} than in previous experiments were found. The origin of these unexpected pressure fluctuations has as yet not been identified with certainty. However, it appears they may be due to normal fluctuations encountered in very low flow conditions with the new pump which required large bypass flows to reduce discharge pressure to values below the test facility design limits. (Note that the replacement pump was an existing pump installed to provide the high flow rates required in these experiments). In a small number of these last experiments, void fraction was found to continue to increase in regions in the divergent part of the test section where the local pressure measured was apparently below the saturation pressure corresponding to T_{in}, acontradictory situation. Small errors in pressure measurement ($\sim$1%) were especially critical in the diverging section of the nozzle where the pressure was almost constant and near the saturation value. These small fluctuations caused the calculational scheme to oscillate between vaporization and condensation.

In the experiments where recondensation occurred, the point where α reached a maximum value should correspond to the location where the liquid crossed the saturation pressure from a superheated state. Examination of the experimental data where saturation crossing was encountered, and calibrations of the pressure transducers and RTD temperature sensors, suggested that an error equivalent of 3 kPa ($\sim$1%) could have been experienced in the last series of experiments.* A correction of + 3.0 kPa was thus applied to the inlet saturation pressure of all runs between 116 and 148 which had the effect of eliminating the few anomalies noted above. This correction was equivalent approximately to increasing the inlet temperature by 1 C, thereby increasing local superheat by an equivalent amount.

The results of two typical calculations, for Exp. 119 and 136, were shown in Figs. 1.1 and 1.2. The values of n, C_Γ and α_o found to give the best fit to the experimental data were summarized in Table It was found that n ranged from 400 to 8000, while C_Γ ranged from 2800 to 8900 m^{-1}. This range of C_Γ compares favorably with the value of $3000 < C_\Gamma < 6300$ m^{-1} found in pipe flows at lower mass fluxes (Reocreux 1974) and reported before (Wu, 1979). The comparison is shown in Figure 1.3.

As was encountered in the case of the straight pipe experiments, when void fractions much in excess of those generally associated with the transition from bubbly to slug (churn) flows were encountered, the model diverged from the experimental results. This indicates the conduction-limited bubble growth model is applicable, as expected, to bubbly flows only and other modeling will be required for churn turbulent and annular or annular dispersed flows.

1.1.2 Comparison with Computer Codes (TRAC-P1A).

The experimental data of five of the runs performed in the third set of flashing tests were also compared with TRAC-P1A predictions. The first three set of data presented in Fig.1.4, 1.5 and 1.6 were performed at 100°C inlet temperatures and increasing mass flow rates from 4.6 - 9.06 kg/s. The second set of the pressure distributions and void profiles presented in Figs 1.7 and 1.8 were

* A recalibration of the RTD, which measures the inlet temperature of the test section, revealed that the temperature indicated was 0.6 C lower than the actual one.

TABLE 1.1

SUMMARY OF COMPARISON OF VOID DEVELOPMENT MODEL WITH BNL EXPERIMENTS

Run*	$C_I (m^{-1})$	α_o	η
119/120	2800	1.1×10^{-6}	1500
122/124	5300	3.7×10^{-6}	400
132/131	3900	1.9×10^{-7}	4000
133/134	8400	4.6×10^{-7}	1000
136/135	6900	2.2×10^{-7}	2000
137/138	5600	3.8×10^{-8}	8000
140/139	5600	3.8×10^{-8}	8000
145/146	8900	1.2×10^{-6}	500
148/147	7400	5.6×10^{-7}	1000

* The first number corresponds to the run in which the pressure distribution was measured. The second number designates the companion void fraction measurement.

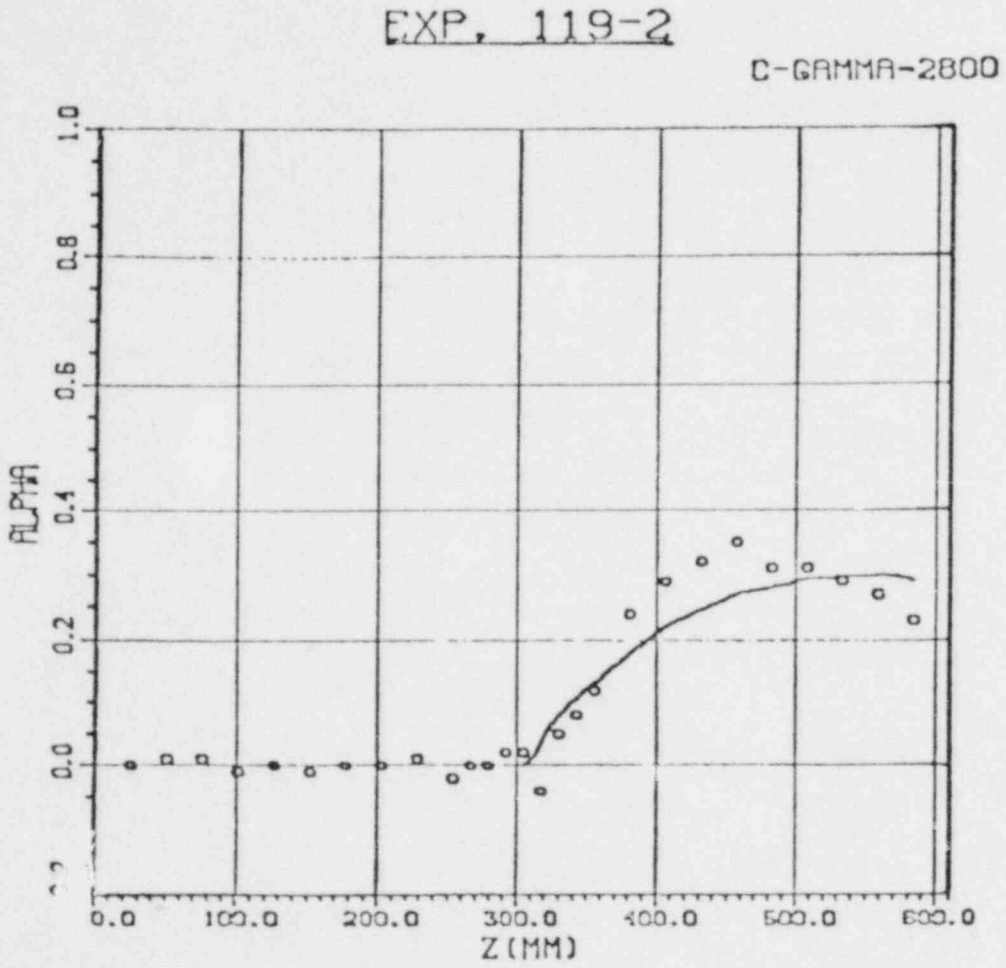

Figure 1.1 Comparison of void fraction distribution predicted by the void development model (curve) and experiment 119/120 (squares).

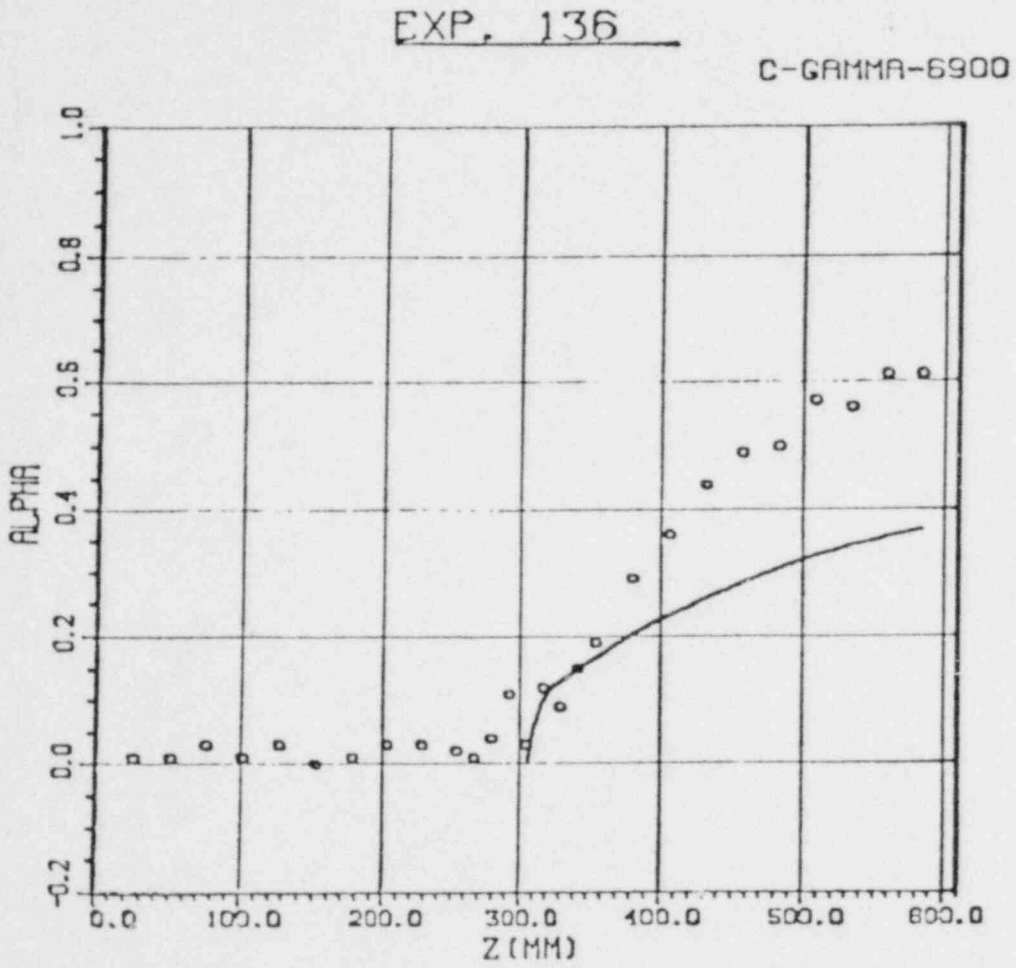

Figure 1.2 Comparison of void fraction distribution predicted by the void development model (curve) and experiment 136/135 (squares).

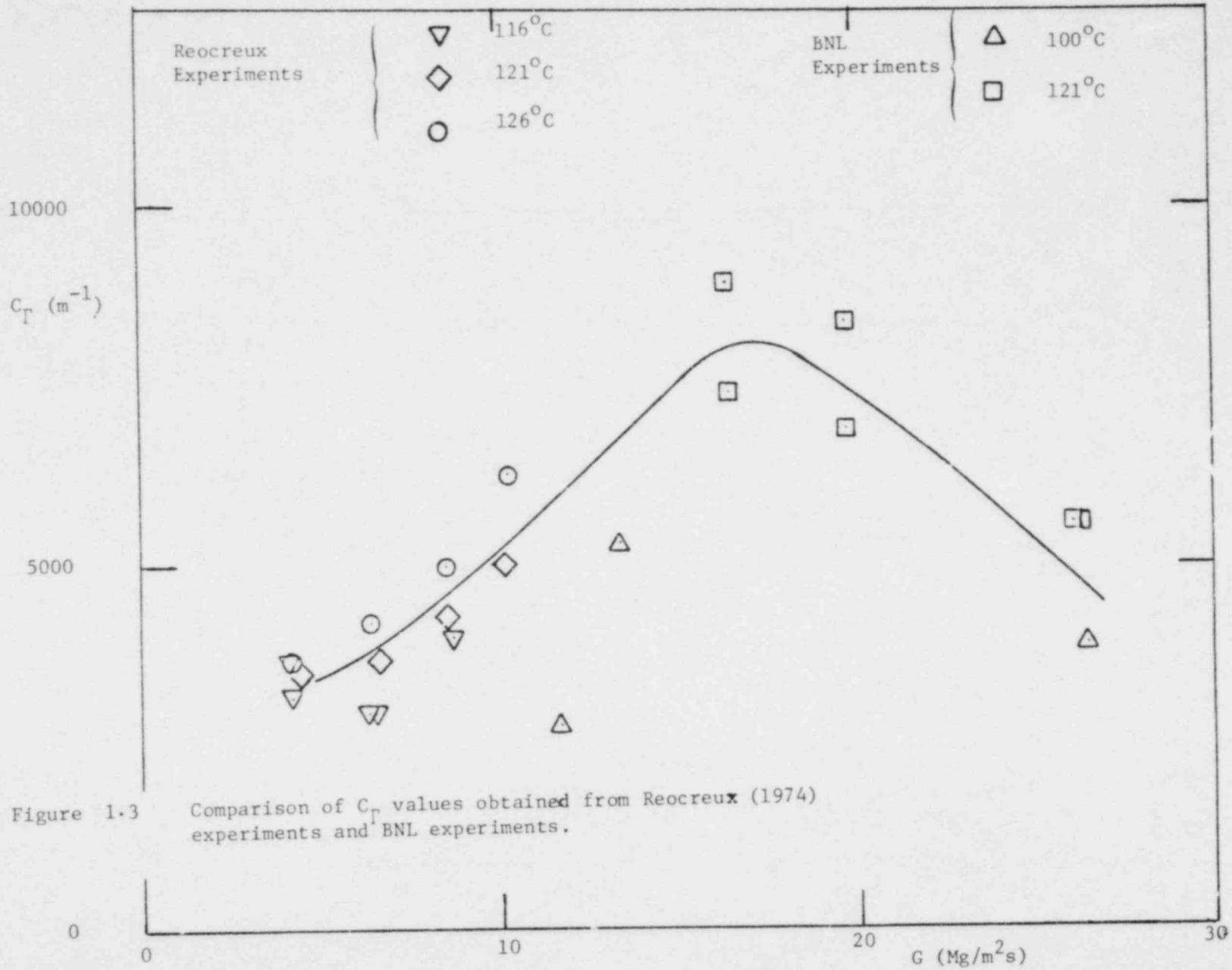

Figure 1.3 Comparison of C_Γ values obtained from Reocreux (1974) experiments and BNL experiments.

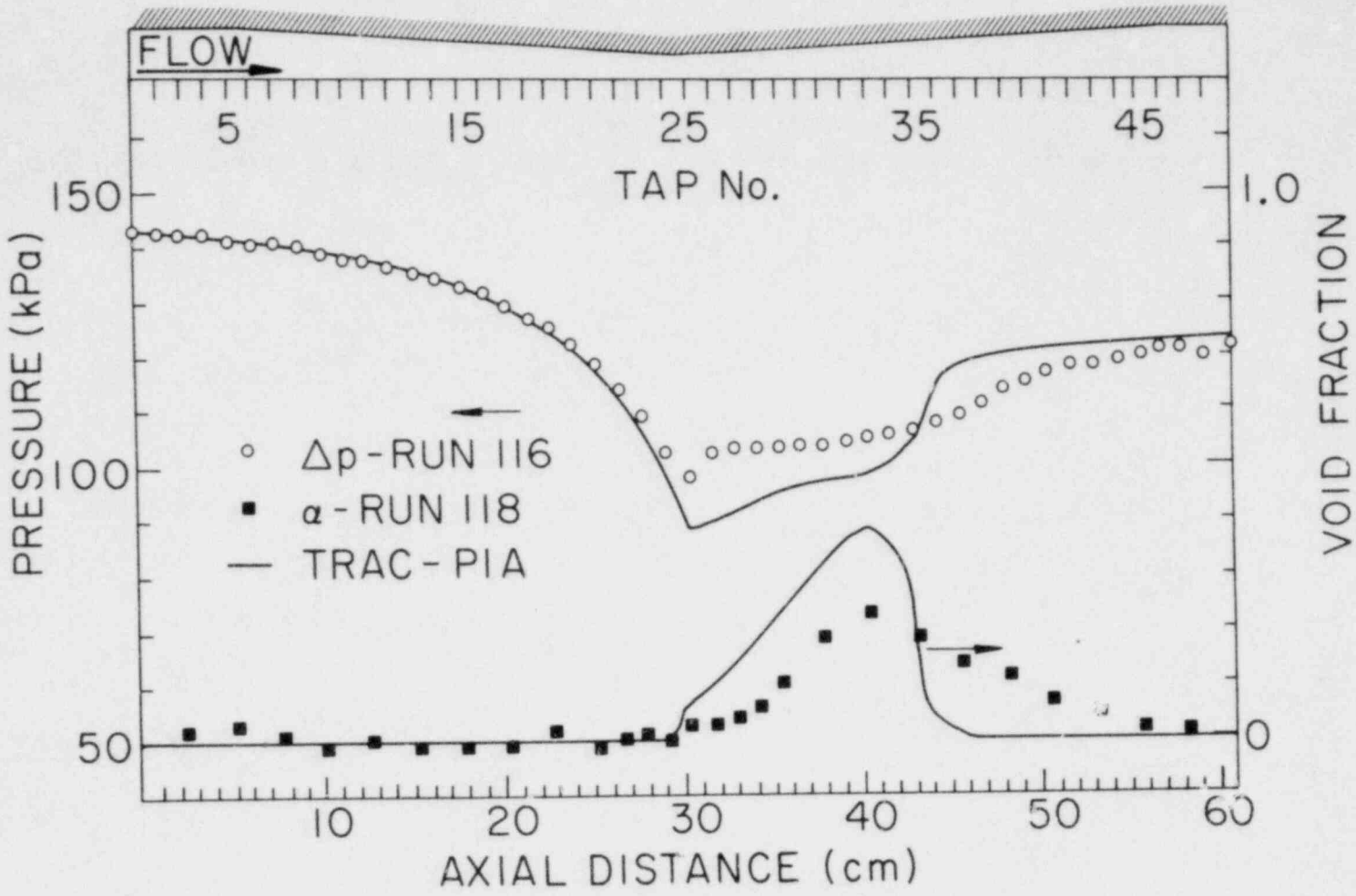

Figure 1.4 Comparison of TRAC-P1A predictions with BNL experimental data for pressure distributions and area averaged void profiles P_{in} = 143 kPa, T_{in} = 99.9 C, G_{in} = 2.28 Mg/m^2 s , p_{ct} = 127 kPa and T_{ct} = 100.4 C ($\dot{m}_{exp}$ = 4.6 kg/s, $\dot{m}_{TRAC}$ = 4.8 kg/s) (BNL Neg. # 2-200-80)

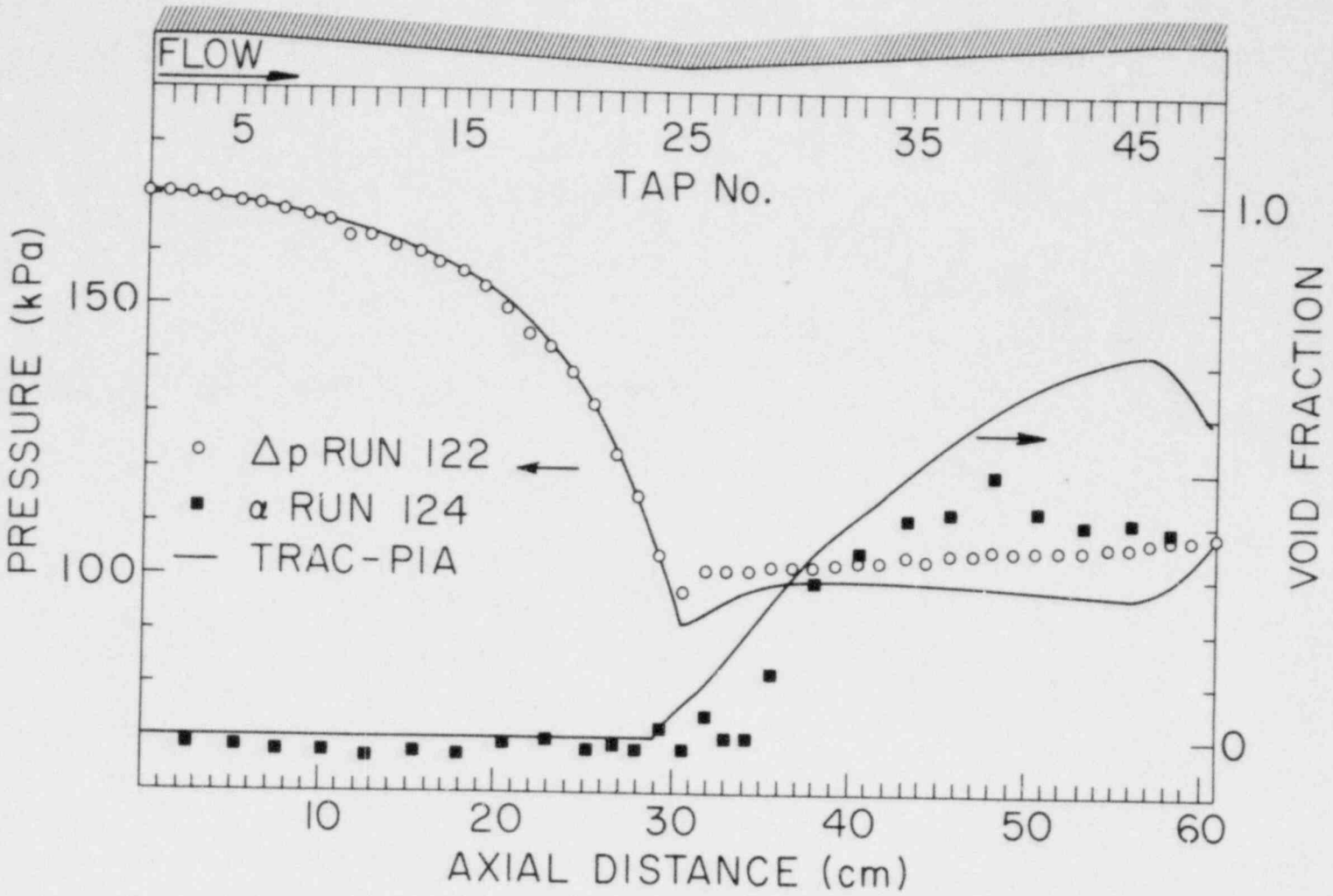

Figure 1.5 Comparison of TRAC-P1A predictions with BNL experimental data for pressure distributions and area averaged void profiles p_{in} = 151 kPa, T_{in} = 100.1C, G_{in} = 2.63 Mg/m^{2}s, p_t = 127 kPa, T_{ct} = 100.5 C ($\dot{m}_{exp}$ = 6.1 kg/s, $\dot{m}_{TRAC}$ = 6.0 kg/s) (BNL Neg. # 2-196-80)

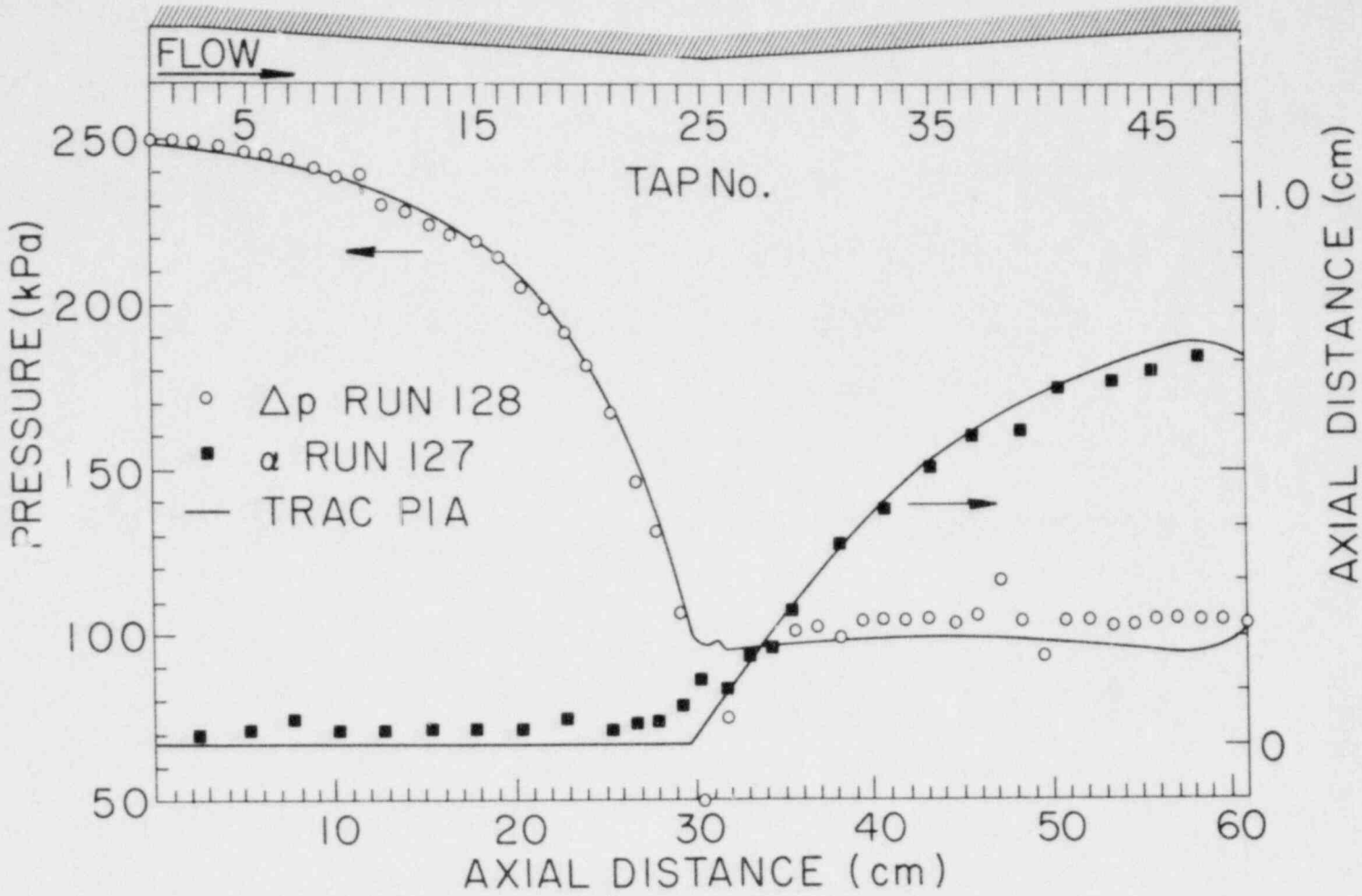

Figure 1.6 Comparison of TRAC-P1A predictions with BNL experimental data for pressure distributions and area averaged void profiles p_{in} = 248 kPa, T_{in} = 100 C, G_{in} = 4.49 Mg/m^{2}s, p_{ct} = 127 kPa, T_{ct} = 100.5 C ($\dot{m}_{exp}$ = 9.1 kg/s, $\dot{m}_{TRAC}$ = 8.6 kg/s)

(BNL Neg. # 2-197-80)

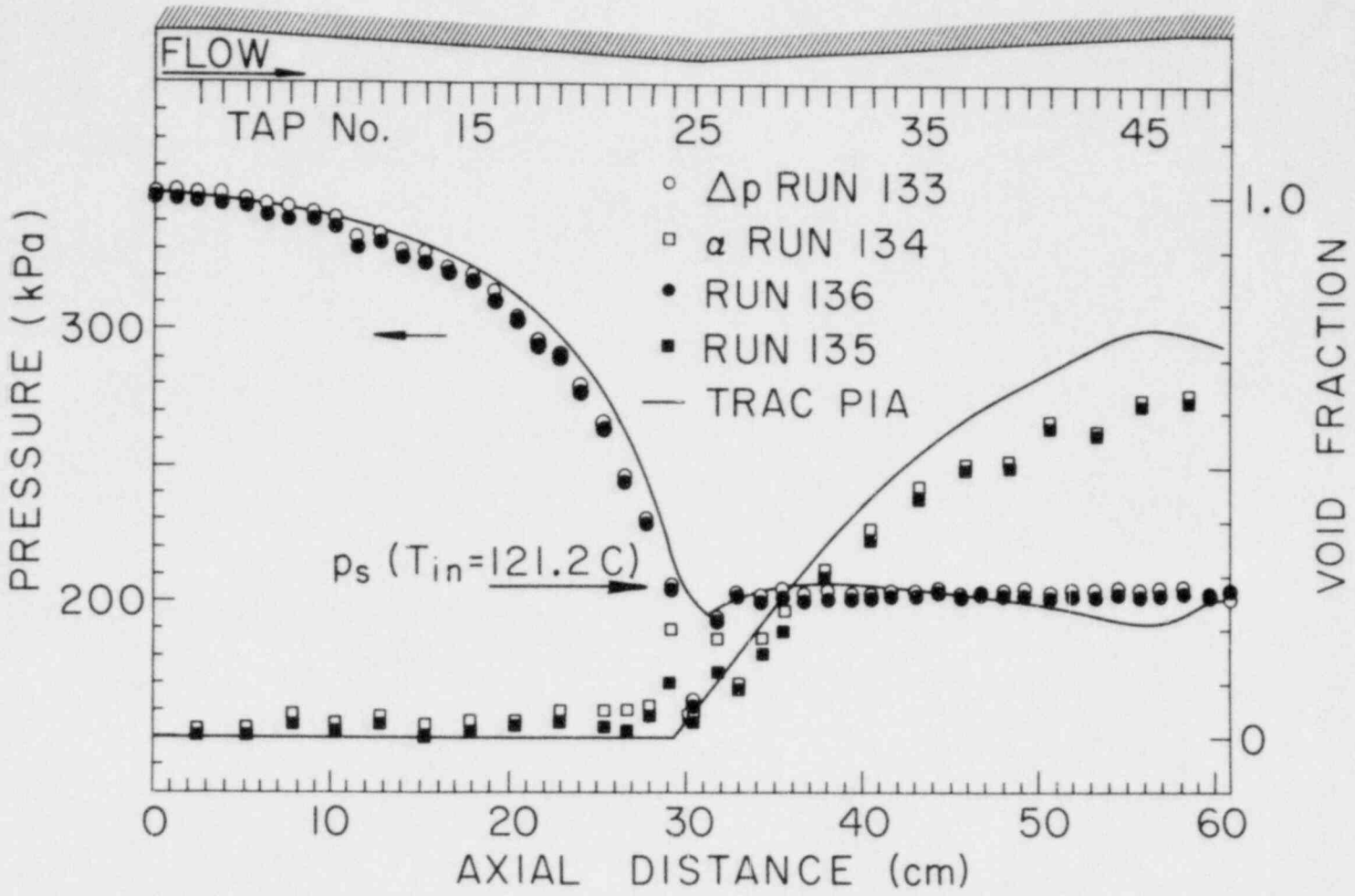

Figure 1.7 Comparison of TRAC-P1A predictions with BNL experimental data for pressure distribution and area averaged void profiles p_{in} = 349 kPa, T_{in} = 121.2 C, G_{in} = 443 kg/m^{2}s, p_{ct} = 233 kPa, T_{ct} = 121.7 C($\dot{m}_{exp}$ = 8.9 kg/s, $\dot{m}_{TRAC}$ = 8.4 kg/s) (BNL Neg. # 2-199-30)

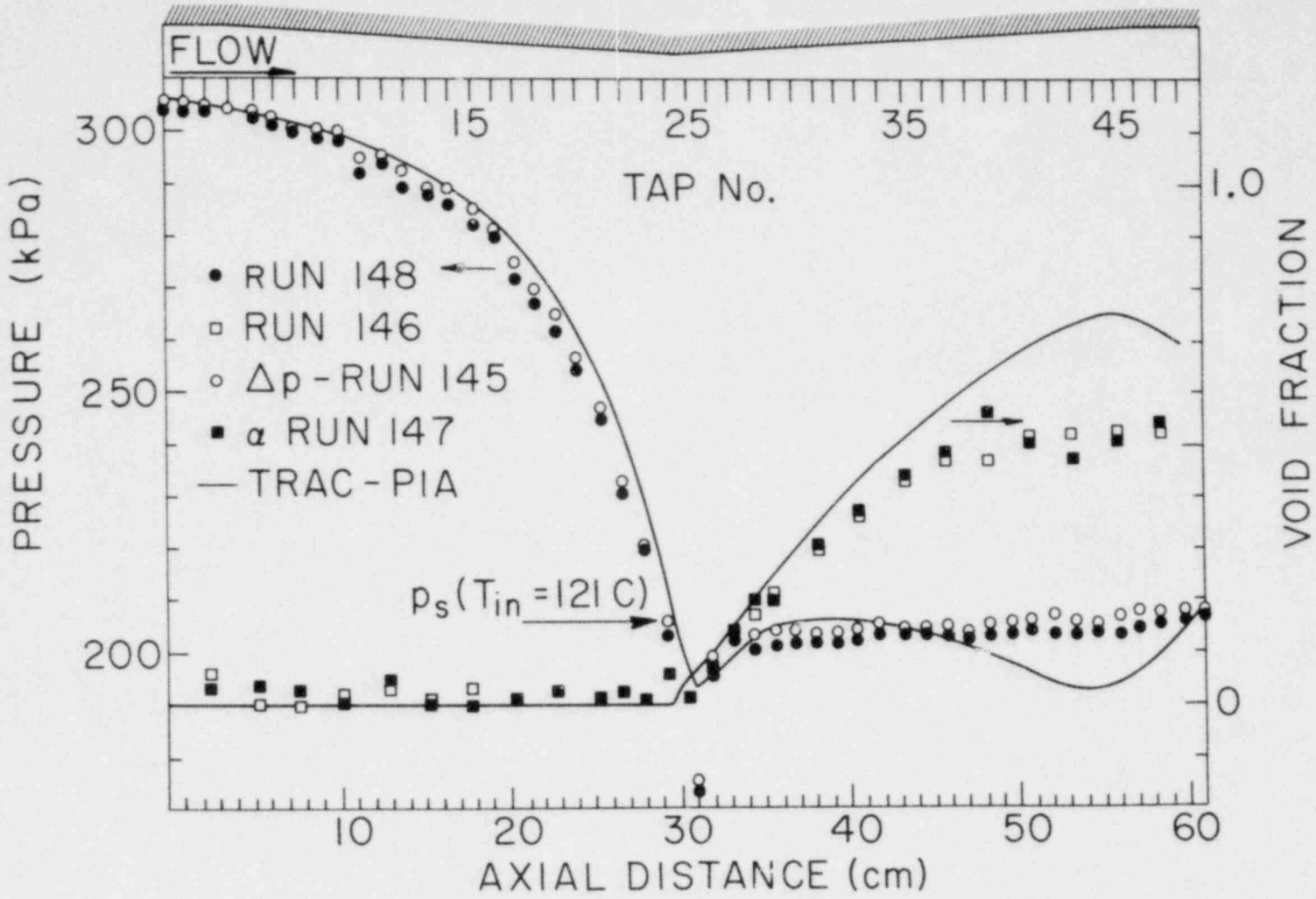

Figure 1.8 Comparison of TRAC-P1A predictions with BNL experimental data for pressure distributions and area averaged void profiles $p_{in} = 305$ kPa, $T_{in} = 121.2$ C, $G_{in} = 3.7$ Mg/m^{2}s, $p_{ct} = 234$ kPa, $T_{ct} = 121.7$ C($\dot{m}_{exp} = 7.5$ kg/s, $\dot{m}_{TRAC} =$ kg/s)

(BNL Neg. # 2-198-80)

conducted at an inlet temperature of 121 C and mass flow rates of 7.4 and 8.9 kg/s.

The observations from the comparison are similar to the ones reported before; that TRAC-P1A predicts a lower mass flow rate than the experimentally measured ones for the last three cases. It predicts the trends in the pressure and void profiles. In all these Figures,1.4,1.5,1.6,1.7 and 1.8 the void fractions plotted at a given cross section are the area averaged values calculated from the transverse profiles obtained at each axial location.

The last two figures, 1.7 and 1.8,representing the two repeats of the pressure and void profiles that are performed for each run depict an example of the reproducibility and repeatability of the results.

REFERENCES

ABUAF, N. and WU, B. J. C., Reactor Safety Programs Quarterly Progress Report for the Period July-Sept. 1979, BNL-NUREG- (1979).

ALAMGIR, Md. and LIENHARD, J.D., Personal communication (1979), J. of Heat Transfer (in press).

FORSTER, H. K. and ZUBER, N., "Growth of a Vapor Bubble in a Superheated Liquid," J. of Appl. Physics, Vol. 25, 4, pp. 474-478 (1954).

JONES, O. C., Jr. and ZUBER, N., "Evaporation in Variable Pressure Fields," paper No. 76-CSME-(SChE-123. Nat. Ht. Tran. Conf. (1976) and Trans. ASME, J. Heat Trans., 100 Cm, p. 453-459 (1978).

OSWATITSCH, K., "Kondensation serscheinungen in Uberschalldusen," Z. angew.

PLESSET, M. S. and ZWICK, S. A., "The Growth of Vapor Bubbles in Superheated Liquids," J. of Appl. Physics, Vol. 25, 4, pp. 493-500 (1954).

REOCREUX, M., "Contribution a 1'etude des Debils Critiques en Ecoulement Diphasique Eau-Vapeur," PhD. Thesis, Universite Scientifique et Medicale de Grenoble, France (1974).

SAHA, P., Reactor Safety Programs Quarterly Progress Report for the Period, April-June 1977, BNL-NUREG-50683, p. 145 (1977).

WEGENER, P. P. and WU, B. J. C., "Gasdynamic and Homogeneous Nucleation in Nucleation Phenomena," A. C. Zettlemayer, Ed., p. 325, Elserier, N.Y. (1977).

WU, B. J. C., SAHA, P., ABUAF, N., and JONES, O. C., Jr., "A One-Dimensional Model of Vapor Generation in Steady Flashing Flow," BNL-NUREG-25709 (1979).

WU, B. J. C., "Analysis of Condensation in the Centered Expansion Wave in a Shock Tube," Condensation in High-Speed Flows, A. A. Pouring, Ed., ASME, 1977.

ZIMMER, G., WU, B. J. C., LEONHARDT, W. J., ABUAF, N., and JONES, O. C., Jr., "Pressure and Void Distributions in a Converging-Diverging Nozzle with Vapor

Generation," BNL-NUREG-26003 (1979).

ZUBER, N., STAUB, F. W., and BIJWAARD, G., "Vapor Void Fraction in Subcooled Boiling and in Saturated Boiling Systems," Proc. 3rd Int. Heat Transfer Conf. 5. p. 24 (1966).

2. RAMONA, IRT and RETRAN Code Modification and Evaluation

The BNL jet pump-recirculation loop model, which was recently added to the code, is being modified so that the jet pump M ratio can be specified as an input number. Two approaches are being tried. In one, the given M ratio is used and the core inlet loss coefficients are adjusted to give the expected steady state jet pump head, and mass flow. In the other approach, the loss coefficients are fixed and the jet pump head takes on some value in order to give the correct mass flow. A new jet-pump-recirculation loop and steam separator model developed by Scandpower (ScP) was received.

A new ScP fuel rod model was received and implemented. The calculated core power during Turbine Trip Test No. 3 (TT3) with this model in place is now in better agreement with the measured data. Nineteen different trips have now been implemented into the code.

Code Assessment continues with comparisons being made against data from TT3 and data calculated by the BNL-TWIGL code. Transfer function calculations based on a sinusoidal disturbance indicate the void response to a pressure increase is not as large as expected. Changes in the slip model did not change the power response for TT3 significantly; nor did changing the initial core average void fraction. Problems in achieving the steady state were investigated as were problems which result in unexpected oscillations in the steamload and the inability to have direct energy deposition in the moderator. Work continued on implementing the steamline model and in writing routines which produce a plot-file.

2.1 RAMONA Jet Pump - Recirculation Loop Model

Work continued with the BNL jet pump-recirculation loop model in order to have the jet pump M ratio as a given input number. To do this the hydraulics input for the Peach Bottom Turbine Trip Test No. 3 (TT3) was modified by reducing the core loss coefficients. Then the input of the M ratio and proper suction leg and drive line jet pump loss coefficients resulted in the correct steady state mass flow and a jet pump head equal to that obtained using RELAP-3B, Lu (1979).

The jet pump M ratio is defined as

$$M_R = W_s/W_d$$

where W_S and W_d are the suction leg and drive line mass flows, respectively. Conservation of mass yields

$$W_{RL} = W_s + W_d \quad .$$

The given total recirculation line mass flow, W_{RL}, then allows calculation of the suction and drive flows

$$W_s = W_{RL}/(1+M_R)$$

$$W_s = W_{RL} - W_d \quad .$$

Then for a given jet pump head, Equations (5) and (8) of Ruger (1979) can be used to obtain the suction leg loss coefficient:

$$K_{sct} = \Delta P_{jet} + \Delta P_{dif} - \frac{W_s^2}{2\rho_m A_{sct}^2} - \Delta P_{PUMP}$$

where P_{jet} and P_{dif} are given by Equations (6) and (7) of Ruger (1979). The total drive line loss coefficient can be obtained from the drive line momentum equation, Equation (10) of Ruger (1979), under steady state conditions.

$$K_D = K_d + K_{dwn} + K_{noz}$$

$$= \left[\Delta P_{dp} + \left(K_{sct} + \frac{1}{2\rho_m A_{sct}^2}\right) W_s^2\right] / W_d^2 - \frac{1}{2\rho_m A_{noz}^2}$$

The steady state tuning is then concluded by adjusting the RAMONA core inlet loss coefficients such that the given jet pump heat produces the desired steady state mass flow.

This steady state tuning was accomplished outside the code and the resultant pump loss coefficients were then used as input data. This procedure is presently being incorporated into the RAMONA code along with an alternate procedure in which the RAMONA core loss coefficients remain fixed and the jet pump head is tuned to give the desired steady state mass flow. The relative usefulness of these procedures will be tested on Peach Bottom Turbine Trip Tests 1 and 2.

The transient behavior of the jet pump-recirculation loop model has been further tested by a pump trip calculation in which the drive pump is cut off during the transient. This case led to the discovery of some coding errors in the drive pump head calculations, which were not evident under the Peach Bottom Turbine Trip Test 3 conditions, since pump response was small in this case. These errors have been corrected resulting in a smooth coast down pump trip calculation.

The Scandpower (ScP) jet pump-recirculation loop model and steam separator model were received. The package included documentation and RAMONA updates which will now be applied to the BNL version and tested.

2.2 RAMONA Plant Protection System

Nineteen different trips have now been implemented into the RAMONA III code. They can be broken up into five classifications according to the trip that is possible to activate. These five areas are scram, turbine stop valve trip, recirculation pump trip, turbine bypass valve opening, and feedwater

system trip. A memo describing each of the signals that cause a particular type of trip to occur and the RAMONA input associated with each trip has been written (Lekach (1980)).

Input for the trips adheres to the RAMONA input specifications. Input cards can be put anywhere in the input deck in any order. The default status is no trip unless there is an input card for a particular trip that will activate the analysis of the trip signal. Trips are activated during the dynamic mode of RAMONA calculations. At the beginning of a run all the trip specifications for that run are printed out. During a run, whenever a trip is activated, a message appears. At the end of a run a summary of all trip actions taken appears in the summary section of the printout.

Table I lists all the trips. If a feedwater system trip is called for, a table of flowrate (as a function of flowrate just before the trip) versus time must be input. Similar tables must be input for the flowrates at the turbine stop valve and/or bypass valve if trips for these valves are specified. If scram is possible a control rod speed must be given. Each trip can have a delay time between the trip signal and trip activation.

2.3 RAMONA Fuel Rod Modelling

The new ScP fuel rod model was received and implemented into RAMONA-III. Results at BNL for Sample Problem No. 2 reproduce those obtained by ScP. This model is similar to the BNL model discussed in the previous progress report. They both allow for heat capacity in the clad and for an explicit gap representation but use different numerical algorithms. Non uniform heat generation which is taken into account in the BNL model is not considered in the ScP model. Turbine Trip Test No. 3 was run with the new fuel rod model. The calculated core power during the transient was higher with the new model because the inclusion of clad heat capacity tends to delay the negative feedback which results from the heat being conducted into the coolant from the fuel rod. These results improve the agreement with measurements. The trend was also found to be true using the BNL fuel rod model.

The original BNL fuel rod model only allowed for a total of four nodes for the pellet, gap, and clad. RAMONA-III was modified to allow for more nodes and noding studies were begun. Since there exists another fuel rod model and programming problems related to the BNL model, this work has been deferred.

2.4 RAMONA Code Assessment

Calculations of Turbine Trip Test No. 3 (TT3) show that RAMONA-III underpredicts the rise in power that was observed. The cause for this seems to be a combination of deficiencies in the hydraulics modelling and the neutronics input data. In order to isolate and identify the source of these deficiencies a small sinusoidal pressure peturbation was imposed rather than the TT3 steamdome pressure. All other input was held constant. The system variables such as void, relative power, average flux, etc. were observed and noted to exhibit sinusiodal behavior. Amplitudes and phases were noted and used to compute approximate transfer functions. Of special interest were those of pressure-void and void-power. While realizing all the limitations of using such

TABLE 2.1

RA' ONA PLANT PROTECTION SYSTEM

Trip	Condition
A. Feedwater System Trip	1. Time 2. High vessel water level
B. Scram	1. Time 2. Turbine inlet valve closure 3. High power 4. Low reactor vessel water level 5. High reactor vessel water level 6. High system pressure 7. Main steam isolation valve closure
C. Turbine Stop Valve Trip	1. Time 2. Low vessel water level 3. High vessel water level 4. Low turbine inlet pressure
D. Recirculation Pump Trip	1. Time 2. Turbine inlet valve closure 3. High system pressure 4. Low vessel water level
E. Turbine Bypass Opening	1. Time 2. Turbine inlet valve closure

analysis on non-linear systems, these approximate numbers were compared to similar numbers extracted from BNL-TWIGL for TT3. Preliminary results indicate agreement in the void-power transfer function. Other relationships noted such as a phase lag between relative power and average flux are to await further study.

The sensitivity of RAMONA to the slip formulation was explored. The replacement of the slip model with the model of Henry-Fauske was attempted but led to difficulty in successfully relaxing to a steady state. Removing "slip" by modifying the parameters in the Bankoff-Malnes correlation and allowing the stagnation vapor velocity to approach zero void worked successfully. It increased the relative power peak by 10%.

The sensitivity of relative power peak to the steady state average void in the core was explored. Different steady states were obtained by varying the flow through the core thereby obtaining a variety of mean core voids. The BNL-TWIGL value for mean core void was lower than the RAMONA value (0.28 as opposed to .34). Such variation made less than 10% difference in the relative power peak value.

Specific problems related to using the code were investigated. These included problems in achieving the steady state, oscillations in the steam-load, and errors in the direct moderator energy deposition.

The RAMONA code has shown to be sensitive in attempts to relax to steady state. The steady state formulation will not entertain negative velocities. When negative velocities are encountered they lead to fatal errors. During the relaxation process swings in values do occur which often prevent successful relaxation to steady state. One example of this sensitivity was in a study in which the input data for the Solberg void correlation was varied. Small variations in these parameters led to an unsucessful relaxation of the steady state. This has also been observed with changes in downcomer/recirculation loop input parameters.

The mass flow into the steam line, WSL, was observed to oscillate. In TT3 WSL of course changes magnitude and sign consistent with acoustic waves in the long steam line. In the version of RAMONA used, the value of WSL was noted to swing in one time step from positive to negative its full value. In this version the steam dome pressure is imposed from a data table. (A series of ordered pairs of pressure and time values.) The value of the derivative of pressure with time is computed from the table and is discontinuous. In this version of the code the value of WSL is computed from this derivative, the volume of vapor in the vessel and its compressibility. Calculations with this part of the code were modified and were not found to affect the power peak. This area of RAMONA will be modified when the BNL steamline model is incorporated.

Turbine trip test results have been found in the past to be sensitive to the amount of power directly deposited in the water of the reactor. RAMONA considers the inchannel water as "coolant" and the water in the bypass region

as "moderator." The bypass region includes water in the gaps between bundles as well as in the reflector region. Direct neutronic feedback is only affected by the coolant conditions; the moderator temperature and density are not used in that way. Nevertheless the overall system balance requires the proper moderator conditions. Seven input numbers in RAMONA bear on the energy deposited outside the fuel. In examining how these were used it was discovered that the code did not deposit energy directly in the moderator as advertised. The only mechanism for energy deposition in the moderator was by conduction from the coolant region.

2.5 RAMONA Programming Considerations

Work has continued on the implementation of the steamline model in RAMONA-III and is now close to completion. With the additional code and storage required for the steamline model the BNL version of RAMONA-III is now close to the capacity of Small Core Memory on the BNL 7600. Before the implementation of other changes and new models to the code it will be necessary to create an overlayed version of RAMONA-III.

Preliminary ordinate-abscissa plots have been produced from information generated by RAMONA. The plotting program expects RAMONA to produce a single record at each output time which must be preceded by header information at the beginning of the plot file. In RAMONA not all variables are in memory at the same time, different parts of the calculation are carried out with differing time steps, and rejecting/repeating of steps is allowed. The code has been written and implemented to allow an easy mechanism to output information to the plot file. Calls to output specific variables to the plot tape can be done locally in the routines the variables are referenced with heading information being generated automatically.

2.6 IRT Code Modification and Evaluation

2.6.1 Once-Through Steam Generator Modeling - Mark I Version

The Mark I version of the once-through steam generator (OTSG) model that has been implemented in the IRT code is based on assumptions similar to the IRT primary system modeling (i.e., homogeneous equilibrium model with the system pressure spacially constant). The steam generator secondary side is divided into 13 control volumes with the 12th volume representing the upper annular space connecting the secondary side to the steamline. The 13th volume is used to represent the downcomer and includes a provision for the addition of normal feedwater. For each of the secondary side volumes, excluding those representing the annular steam space and the downcomer, there are corresponding primary side and tube metal volumes that are used for the calculation of the steam generator heat transfer rate. Between one of the secondary side nodes and the downcomer, there is a path (to represent the aspirator) through which a fraction of the steam in the tube region is recirculated to the downcomer to preheat the feedwater to approximately saturated conditions. The pressure in the primary system steam generator volumes is assumed uniform spatially as calculated by the original IRT equations. The secondary side pressure is also spatially uniform and is calculated from the conservation of mass and energy equations and the equation of state. The flow from the downcomer to the secondary tube region is strongly dependent on friction and the difference in gravity head between the downcomer and boiling region and is obtained by solving the momentum equation (assuming a uniform secondary side pressure).

A provision has been included for the addition of auxiliary feedwater that is distributed over a fixed number of nodes in the upper tube region of the secondary side. Alternatively, auxiliary feedwater can be added to the downcomer in the same way as normal feedwater.

The boundary conditions for the primary side volumes include coolant enthalpy and flow rate at the primary side steam generator inlet. These parameters are obtained from the IRT primary system calculation. The secondary side boundary conditions include the feedwater flow rate and enthalpy; the steam flow removed from the secondary side is either user specified or calculated from the OTSG model secondary side control system.

Each of the steam generator tube nodes is assumed to be at a uniform temperature at the centerline of the tube wall. The secondary side surface wall temperature, required in calculating the heat transfer coefficient, is estimated from the average tube temperature by accounting for the tube internal heat transfer resistance. The primary and secondary side heat transfer coefficients are determined based on the thermal-hydraulic conditions prevailing in each control volume. The heat transfer modes available include forced convection, subcooled and nucleate boiling, transition boiling, stable film boiling and single-phase steam flow. In addition, correlations for the onset of boiling and critical heat flux are provided.

This model will be available in each of the primary system loops such that asymetric primary and secondary system plant transients can be simulated.

2.6.2 Once-Through Steam Generator Modeling - Mark II Version

The current once-through steam generator model in the IRT code consists of 12 fixed volumes for each of primary, secondary tubes and metal wall, therefore needing 36 calculational volumes. It is suggested that moving boundary scheme, requiring much fewer nodes, may save calculation time and also alleviate instability problems due to sudden change of heat transfer regimes in a large fixed volume.

The suggested (moving boundary) model divides the secondary side tube of the steam generator by up to four boundaries including two moving boundaries. The fixed boundaries may be set at the points of tube rupture and recirculation to downcomer as prescribed by user input. The moving boundaries divide the liquid or vapor regions from the two-phase region and are tracked throughout the calculation. All four boundaries may not exist at all times.

The primary side is considered to be entirely liquid or low quality two-phase region, consistent with the current IRT code. The boundary between liquid and two-phase regions in the primary side is not tracked because it is not considered as important as in the secondary side for the range of problems that the IRT code is used. Tracking both primary and secondary boundaries seems to make the program logic much more difficult without corresponding benefit.

As with the current IRT code, the boundary conditions are provided by the IRT primary loop calculation (h_{in}, W_{in}, p) for primary side and user provided function (h_{in}, W_{in}, W_{out}) for the secondary side. In both sides, pressure is assumed to be spatially uniform. The original IRT assumption of homogeneous and equilibrium is retained. The possibility of flow reversal is not considered.

The analysis is based on a transient, one-dimensional, homogeneous equilibrium model. Two conservation equations of mass and energy are integrated over the variable volume to obtain two ordinary differential equations expressing the rate of change of average density and enthalpy in each region. Since flow rates are provided as part of boundary conditions for the both sides, the momentum equation will not be solved. After some manipulation of these integrated equations, one obtains the secondary side overall mass conservation equation:

$$\left[\sum_{i=1}^{n} \frac{V_I}{v_{i+1} - v_i} \left\{ \left(\frac{1}{v_{i+1}} - \langle\rho\rangle_I \right) \left(\frac{\partial v}{\partial p} \right)_h \Bigg|_{i+1} - \left(\frac{1}{v_i} - \langle\rho\rangle_I \right) \left(\frac{\partial v}{\partial p} \right)_h \Bigg|_{i} \right\} \right] \dot{p}$$

$$+ \sum_{i=1}^{n} \frac{V_I \beta_I}{v_{i+1} - v_i} \left(\frac{1}{v_{i+1}} - \langle\rho\rangle_I \right) \dot{h}_{i+1} - \sum_{i=1}^{n} \frac{\beta_I V_I}{v_{i+1} - v_i} \left(\frac{1}{v_i} - \langle\rho\rangle_I \right) \dot{h}_i$$

$$+ A \sum_{i=2}^{n} \left(\langle\rho\rangle_{I-1} - \langle\rho\rangle_I \right) \dot{Z}_i = W_1 - W_{n+1} \qquad (1)$$

where subscript I indicates quantities associated with i-th zone and i with i-th boundary.

Similarly, the secondary side energy conservation equation is:

$$\sum_{i=1}^{k} \frac{V_I}{\beta_I} \frac{1}{v_{i+1} - v_i} \left[\left\{ \beta_I (h_i - h_{k+1}) - v_i \right\} \left\{ \left(\frac{1}{v_{i+1}} - \langle\rho\rangle_I \right) \left.\frac{\partial v}{\partial p}\right|_{i+1} - \left(\frac{1}{v_i} - \langle\rho\rangle_I \right) \left.\frac{\partial v}{\partial p}\right|_i \right\} \right.$$

$$\left. - \left\{ v_i \left(\frac{1}{v_i} - \langle\rho\rangle_I \right) \left.\frac{\partial v}{\partial p}\right|_{i+1} - v_{i+1} \left(\frac{1}{v_{i+1}} - \langle\rho\rangle_I \right) \left.\frac{\partial v}{\partial p}\right|_i - \beta_I \left(v_{i+1} - v_i \right) \right\} \dot{p} \right]$$

$$+ \sum_{i=1}^{k} V_I \left\{ \frac{\beta_I (h_i - h_{k+1}) - v_i}{v_{i+1} - v_i} \right\} \left\{ \left(\frac{1}{v_{i+1}} - \langle\rho\rangle_I \right) \dot{h}_{i+1} - \left(\frac{1}{v_i} - \langle\rho\rangle_I \right) \dot{h}_i \right\}$$

$$+ A \sum_{i=2}^{k} \left\{ \left(\langle\rho h\rangle_{I-1} - \langle\rho h\rangle_I \right) - h_{k+1} \left(\langle\rho\rangle_{I-1} - \langle\rho\rangle_I \right) \dot{Z}_i + A \left(\langle\rho h\rangle_K - \langle\rho\rangle_K h_{k+1} \right) \dot{Z}_{k+1} \right.$$

$$= W_1 \left(h_1 - h_{k+1} \right) + \sum_{i=1}^{k} \langle Q\rangle_I V_I \quad , \qquad k = 1, n \tag{2}$$

(subscript s, denoting secondary side, is omitted for convenience).

In deriving the equations, an assumption is extensively utilized that the distribution of enthalpy, and consequently of specific volume, is linear.

Additional equations will be provided by proper definitions of boundaries.

If fixed boundaries:

$$\dot{Z}_i = 0$$

If moving boundaries:

$$h_i = h_g \text{ or } h_f$$

$$\Bigg\} \quad i = 2, n \tag{3}$$

Or, equivalently,

$$h_i = \frac{\partial h_g}{\partial p}\,\dot{p} \quad \text{or} \quad \frac{\partial h_f}{\partial p}\,\dot{p}$$

Similar equations can be written to describe the primary side thermal-hydraulics. However, mass conservation equation is not needed since inlet pressure (which is assumed to be uniform) is provided by the primary loop calculation.

Since the primary side is considered to be single homogeneous fluid, similar equations as used in the present model are retained with appropriate modifications accounting for moving boundaries, secondary side phase change, and linear enthalpy profile.

$$\frac{\langle\rho\rangle_k}{z}\left(\dot{h}_{i+1} + \dot{h}_i\right) - \frac{\langle\rho\rangle_I}{z}\,\frac{h_{i+1} - h_i}{Z_{i+1} - Z_i}\left(\dot{Z}_{i+1} + \dot{Z}_i\right)$$

$$= -\frac{W}{A}\,\frac{h_{i+1} - h_i}{Z_{i+1} - Z_i} + \langle Q\rangle_I \qquad I = 1, n$$

(subscripts p's indicating primary side are omitted).

The secondary and primary sides are connected via equations describing wall heat transfer:

$$\rho C_p \delta \left\{\left(Z_{i+1} - Z_i\right)\frac{d}{dt}T_{w,I} - \left(T_{w,I} - T_{w,I-1}\right)\dot{Z}_i\right\}$$

$$= \left(Z_{i+1} - Z_i\right)\left\{U_{P,I}\left(T_{P,I} - T_{w,I}\right) - U_{s,I}\left(T_{w,I} - T_{s,I}\right)\right\}, \quad i = 1, n \qquad (4)$$

Volumetric heat flux for the primary and secondary sides (for the case of circular tube) are:

$$\langle Q\rangle_{P,I} = U_{P,I}\left(T_{P,I} - T_{w,I}\right) * S_I/V_I$$

$$= U_{P,I}\left(T_{P,I} - T_{w,I}\right) * 4/D_P$$

$$\langle Q\rangle_{s,I} = U_{s,I}\left(T_{w,I} - T_{s,I}\right) * 4/D_s$$

$$T_I = T\left(p, \langle h\rangle_I\right) \qquad \text{for p and s}$$

Please note there are 4N equations with 4N unknowns. Those unknowns are:

$\dot{p}_s$, $\dot{h}_{i,s}$ (i=2, n+1), $\dot{Z}_i$ (i=2, n)

$\dot{T}_{w,I}$ (i=1, n) and $\dot{h}_{i,p}$ (i=2, n+1).

The simultaneous differential equations described above are solved by Runge Kutta Method. At the end of each time step, the program will check appearance and disappearance of flow regimes and make necessary adjustments.

2.6.3 Once-Through Steam Generator Analysis

The Mark I version of the once-through steam generator model has been used to analyze an overcooling transient for a typical B&W plant. The transient analyzed is an overfeed transient caused by a failure of the integrated control system that allows the initiation of auxiliary feedwater and the continuation of normal feedwater. The event is initiated by a turbine trip. In addition, when the secondary side system bypass system becomes operational, it is assumed to malfunction and remain open. These assumptions have been selected to maximize the primary system cooldown during the transient. The purpose of the calculations is to determine whether primary system voiding occurs during the transient.

Typical results are shown in Figure 2.1. The results indicate that voiding occurs in the reactor upper head region at approximately 45 seconds after initiation of the transient. Additional analyses have been performed to evaluate various changes to the plant design to reduce the primary system voiding. The following changes have been evaluated:

(a) increased emergency core cooling flow

(b) increased emergency core cooling system initiation pressure

(c) combination of (a) and (b)

(d) reduced scram rod worth

(e) increased pressurizer area

Results obtained thus far indicate that voiding occurs in the reactor upper head region for each of the cases analyzed.

2.7 RETRAN Code Implementation and Verification

The MOD002 of the RETRAN code has been received at BNL and is currently being implemented on the CDC-6600. The main difference between MOD001 and MOD002 are corrections in the non-equilibrium pressurizer model. The modifications improve the convergence of the calculation when the pressurizer is nearly solid or nearly empty. In addition, corrections to the restart capability of the non-equilibrium pressurizer model have been implemented.

Work continued on the implementation of various features of the RETRAN code at BNL. Problems with the restart capability and the graphics program are being investigated.

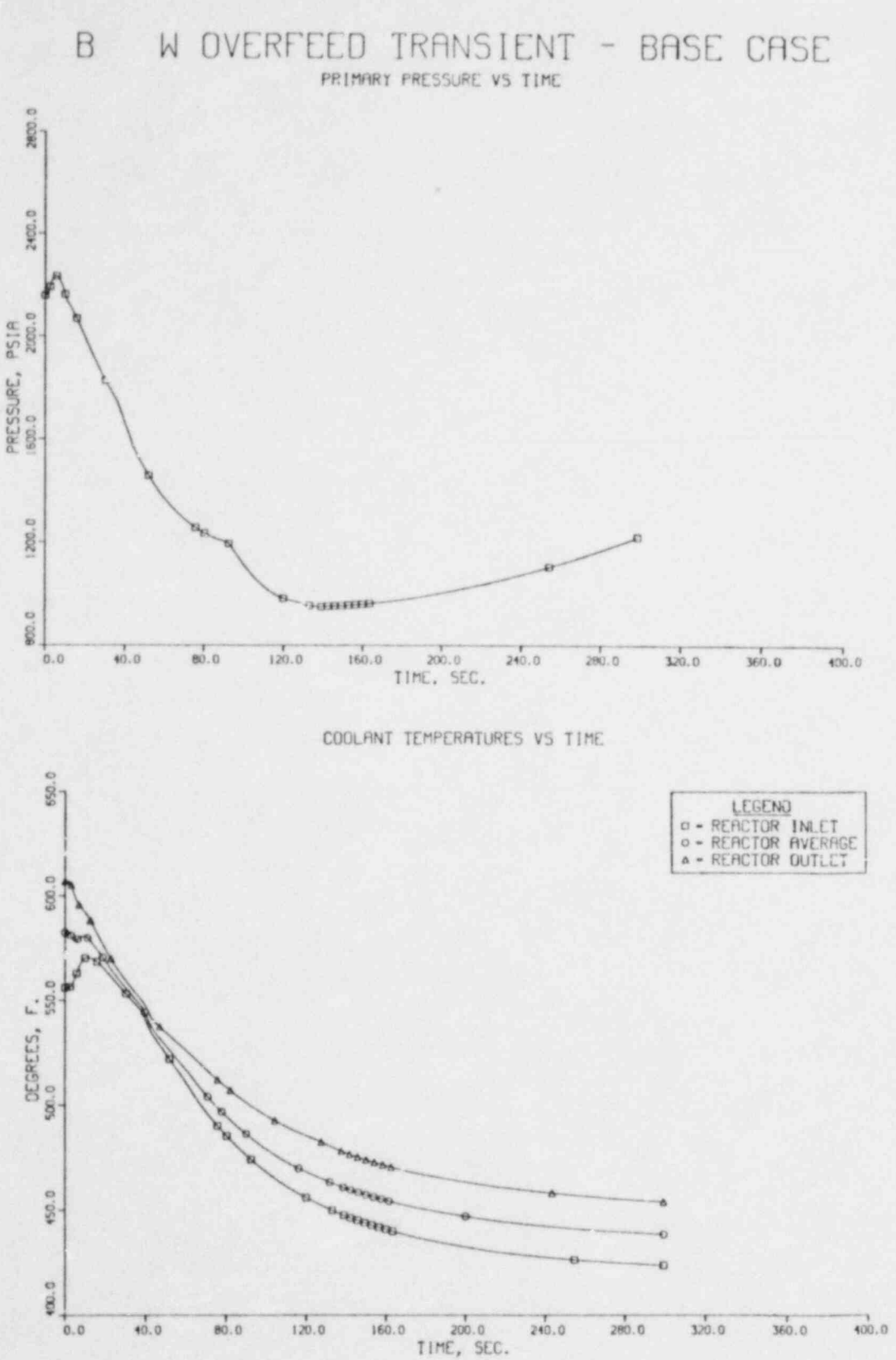
B W OVERFEED TRANSIENT - BASE CASE
PRIMARY PRESSURE VS TIME
PRESSURE, PSIA
2800.0
2400.0
2000.0
1600.0
1200.0
800.0
0.0
40.0
80.0
120.0
160.0
200.0
240.0
280.0
320.0
360.0
400.0
TIME, SEC.
COOLANT TEMPERATURES VS TIME
LEGEND
□ - REACTOR INLET
○ - REACTOR AVERAGE
△ - REACTOR OUTLET
DEGREES, F.
650.0
600.0
550.0
500.0
450.0
400.0
0.0
40.0
80.0
120.0
160.0
200.0
240.0
280.0
320.0
360.0
400.0
TIME, SEC.

Figure 2.1

REFERENCES

LU, M.S., HSU, C.J., CONNELL, H.R., SHIER, W.G., LEVINE, M.M., (1979), "Thermal-Hydraulic Analysis of Peach Bottom-2 Turbine Trip Tests," BNL-NUREG-22526.

RUGER, C.J., (1979) "RAMONA-III Jet Pump Model," BNL internal memo.

LEKACH, S. (1980) "Plant Protection System in RAMONA-III," BNL internal memo.

3. TRAC Evaluation and Model Improvement

3.1 Moby-Dick Nitrogen-Water Experiments (P. Saha)

The TRAC-P1A assessment work with the Moby-Dick nitrogen-water tests (Jeandey, 1979) continued during the reporting quarter. In view of the nodalization study presented in the previous quarterly report (Saha, 1980), all the present runs used 42 cells to represent the test section. A small inlet BREAK component (1 cm long) and twenty moderate-size cells (2 cm long) near the throat were used in all runs. The Mod 1 version of TRAC-P1A was used.

The effect of various two-phase friction factor options available in TRAC-P1A was studied. Sample runs showed a rather large effect of friction factor. Therefore, it was decided to keep the same (experimental) value for the nitrogen flow rate, and then vary the friction factor options. This resulted in different predicted values of the water flow rate for the same test. The predicted flow qualities, calculated from the predicted water flow rates and the input (experimental) nitrogen flow rates, are compared with the experimental values in Figure 3.1. A large effect of friction factor is seen. For both the low and the intermediate qualities, i.e., Run 3176 and 3087, the annular flow model and the Chisholm correlation gave the best predictions. The CISE correlation was the poorest, and both the homogeneous model and the Armand correlation were in between. No converged prediction for the high quality run, i.e., Run 3141, could be obtained. This is probably due to the large difference in slip between the slug and the annular flow regimes (Mahaffy, 1979). An input deck for Run 3141 has been sent to LASL for their examination.

The TRAC predictions for pressure and void fraction for Run 3177 (the only predicted run with void fraction measurement) are compared with the experimental data in Figure 3.2. The annular flow friction factor was used. The predicted pressures near the throat are in reasonable agreement with the data. However, there seems to be an entrance loss which was not modeled in the present calculation. (This can be corrected by specifying an added frictional loss at the entrance or starting the test section somewhat downstream of the entrance.) The predicted void fractions are, however, consistently lower than the measured values, particularly just downstream of the throat. Even for the homogeneous flow, i.e., unity slip ratio, and lower gas densities (corresponding to the slightly lower experimental pressures) the calculated void fractions were not as high as the measured values. Therefore, it seems that the slip ratio has to be less than one! However, it should be noted that with the exception of the first measuring station, all the other void fraction measurements correspond to the diametrical void fraction only. Therefore, the relationship between the diametral (measured) and the area-averaged void fraction must be taken into account before any conclusion can be drawn.

3.2 Marviken Critical Flow Tests (U.S. Rohatgi)

Marviken critical flow test 22 and 24 were recomputed using annular flow option for friction. The results do not change significantly as shown in Table 3.1 So the causes of underprediction of mass flux in the early part of the transient are higher vapor generation rate in the nozzle and the lack of accounting of the heat transfer from the vessel internals and the walls (Rohatgi, 1980a). This heat transfer from the solid boundaries will contribute to vapor generation in

TABLE 3.1 Comparison of TRAC-P1A Predictions of Test 22 with the Homogeneous and the Annular Flow Friction Factor Options.

Time (sec)	P computed/P experimental Homogeneous option	P computed/P experimental Annular option
0	1.0	1.0
0.4	1.1544	1.1542
1.0	0.989	0.99
2.0	0.957	0.958
5.0	0.9401	0.941
10.0	0.9274	0.928
20.0	1.0	1.00
30.0	1.022	1.023
40.0	1.039	1.0395
50.0	1.113	1.114

the vessel and will help in maintaining the pressure. The input for test 22 was modified to compute wall heat transfer and is being debugged.

3.3 Phase Separation Tests (U.S. Rohatgi)

RPI has been conducting phase separation tests in a thin vertical vessel (Rohatgi, 1980b) and TRAC-P1A input was prepared to model this facility. However, the program did not converge to a steady state. This input was further expanded to account for inlet pipe and mixing tee and this simulation also did not converge to a steady state. These input decks have been transmitted to LASL and results are awaited. Meanwhile another variation of this test was tried as a thought experiment. The inlet pipe was closed and the vessel was filled with air/water mixture with a uniform void distribution of 60%. The outlet pipes at the top were kept open. This problem ran for 1036 steps (3 sec real time) in 494 sec CPU time before running out of computer time. However, in this case the phases separated and most of the vapor was in top 4 levels. The initial void distribution and one after 3 seconds are shown in Figure 3.3. The void fraction in top 4 level is close to 1.0 and only level 5 is shown. However, when both the outlet pipes at the top were closed (replace BREAK with FILL), the calculation went up to 1030 steps in 494 sec of computer time. Even after 500 steps, it seems that phases have almost separated.

Above described experiment is for phase separation in the vessel where two fluid model has been used. However, a similar test can be performed with the pipe and modelled as one-dimensional pipe. A pipe of 0.1 m diameter with a length of 6.0 meters is considered. It has 60 uniform size nodes. This pipe is filled with three sets of mixtures (air/water) with varying void fraction distribution. Figure 3.4 shows the final and intermediate void distribution for the case with initial void fraction of 0.75%. The cases with 75% and 50% void distribution, (Figures 3.4 and 3.5) converged to a steady state solution. However, the case with 25% (Figure 3.6) initial void distribution did not converge, even though phases did separate. These single pipe tests show that TRAC-P1A one dimensional formulation can compute counter current flow, low velocity flow and flow separation. These types of computations are important for small breaks where levels are formed.

3.4 FRIGG-Loop Forced and Natural Circulation Tests (L. Neymotin)

A number of computer runs for the FRIGG forced convection test have been made with the steady-state TRAC-P1A option. The input data were corresponding to tests 313007 and 313020. Convergent results have not been obtained despite a wide variation of the numerical scheme parameters (convergence criterion for outer iteration: 10^{-3}-10^{-4}, convergence criterion for vessel iteration: 10^{-4}-10^{-7}, ratio between heat transfer and fluid dynamics time step sizes: 10^{1}-10^{4}, maximum allowable time step size: 10^{-2}-10^{-4}).

An attempt to get a solution to a steady-state air-water two-phase flow problem in a vertical FRIGG-like bundle with the bottom entrance has been also undertaken. The 3D bundle flow region was subdivided into 6 levels in Z-direction and all cross sections had 12 meshes. The lower face of each 1st level's cell has been connected to PIPE and FILL with the flow areas equal to the corresponding area of the vessel mesh. Identical connections with BREAKS

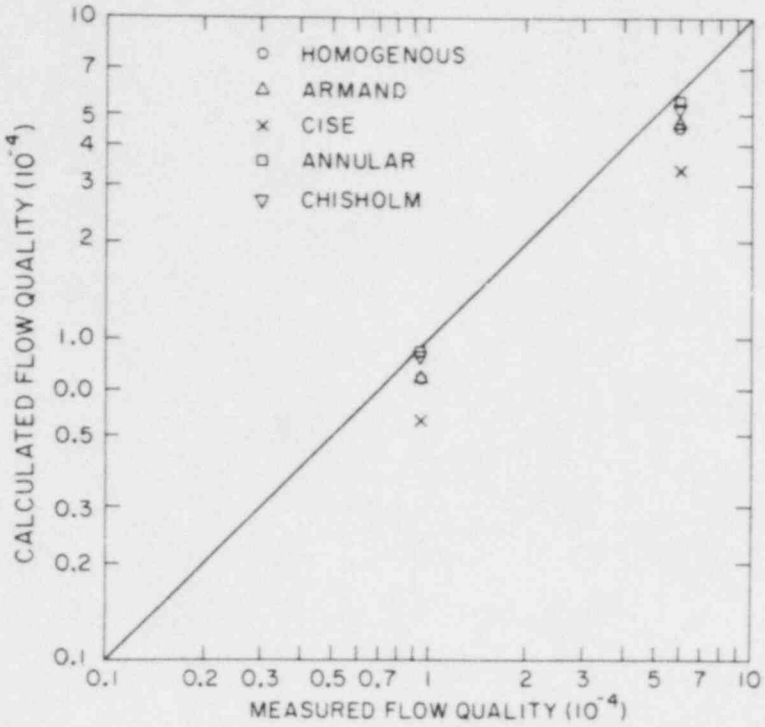

Figure 3.1 Comparison of TRAC-P1A Prediction of Flow Quality with Experimental Data (Run 3176 and 3087). (BNL Neg. No. 1-377-80)

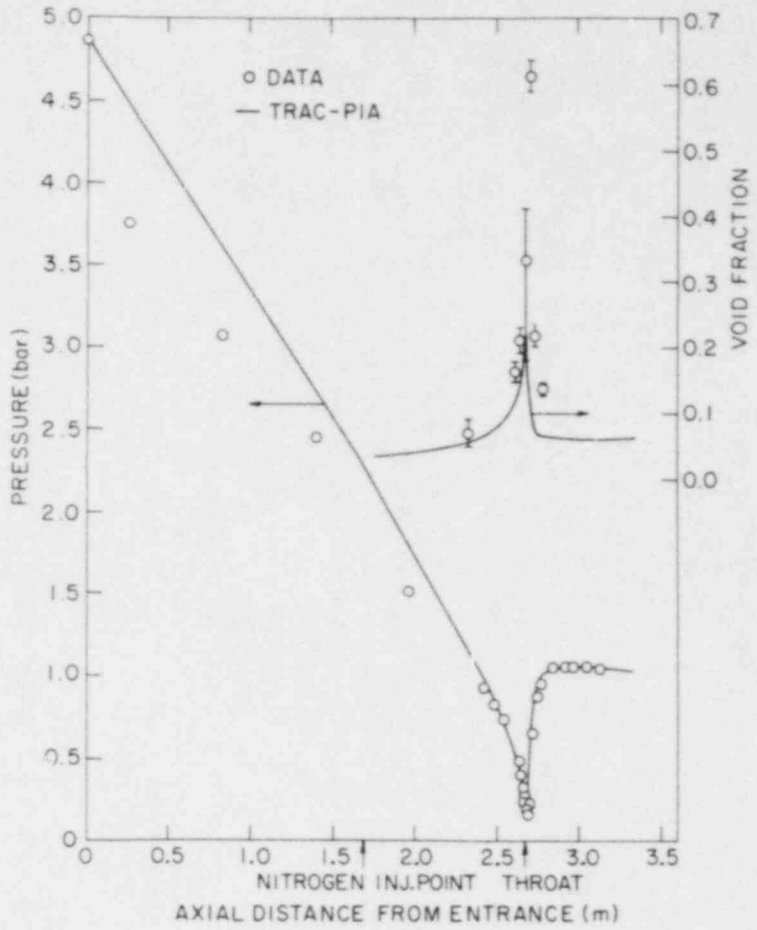

Figure 3.2 Comparison of TRAC-P1A Prediction of Pressure and Void Fraction with Experimental Data (Run 3177). (BNL Neg. No. 1-376-80)

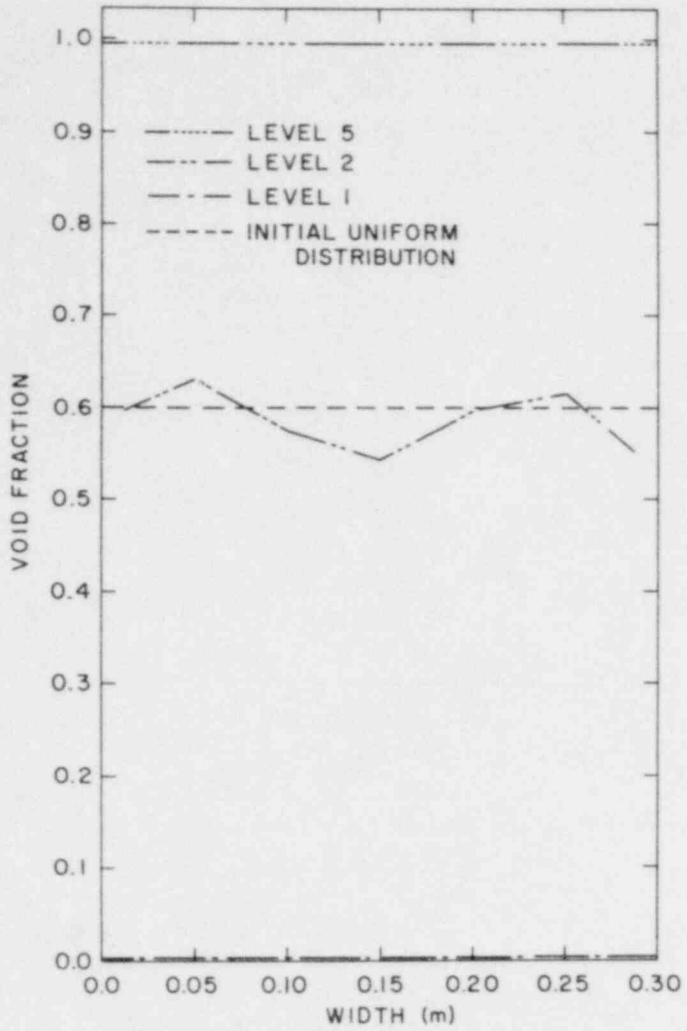

Figure 3.3 Initial and TRAC-P1A predicted void fraction distribution after 1036 steps in RPI 2-D geometry. (BNL Neg. No. 2-544-80)

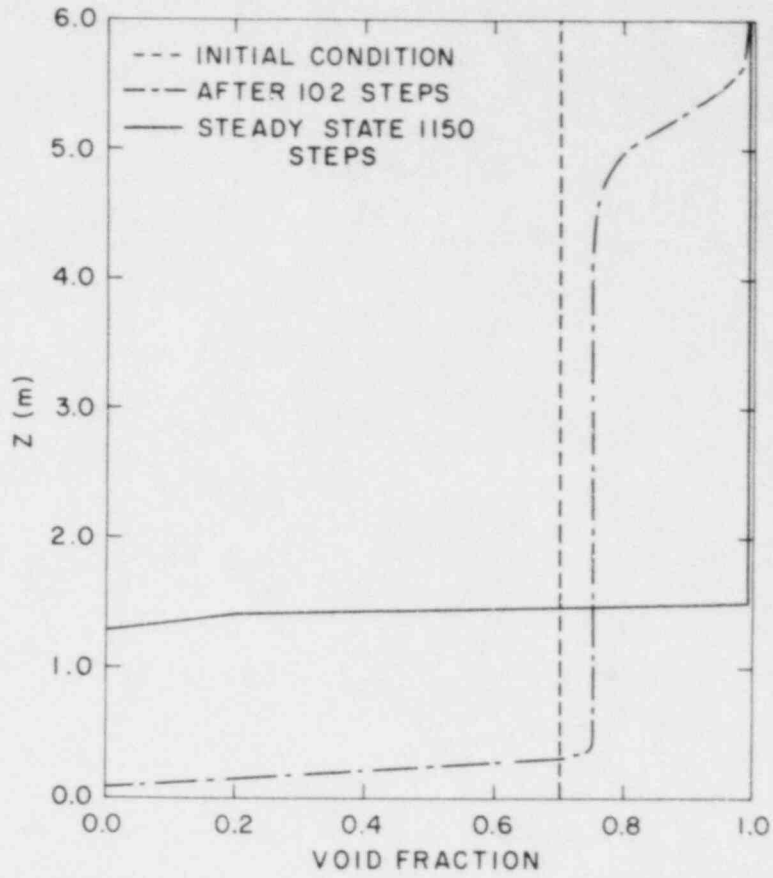

Figure 3.4 Initial, intermediate and final steady state void fraction distribution as predicted by TRAC-P1A for a vertical pipe ($\alpha_{initial}$= 0.75)(BNL Neg No 2-547-80)

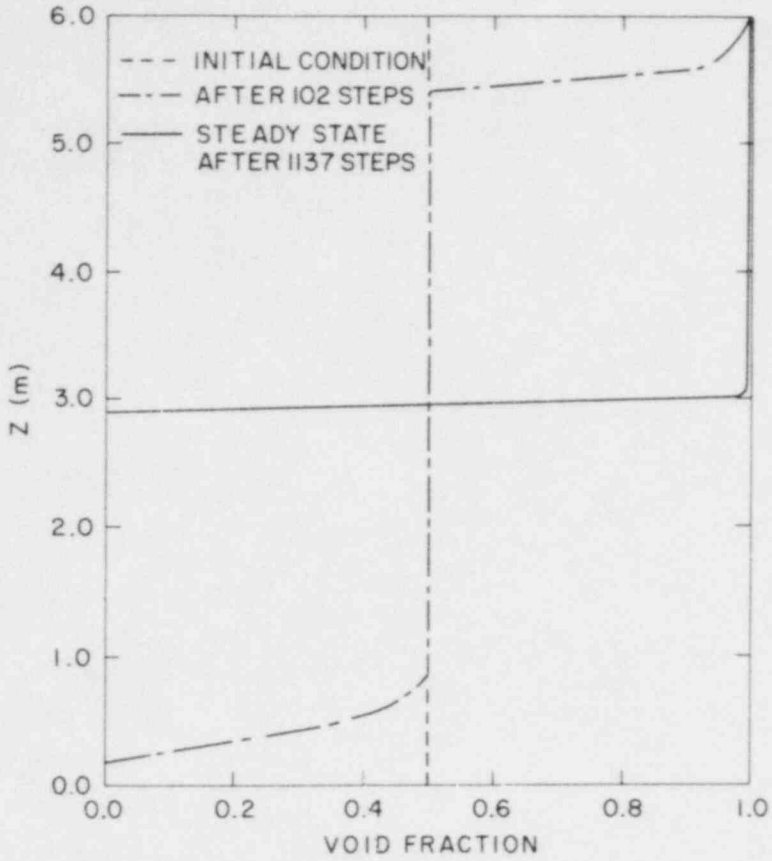

Figure 3.5 Initial, intermediate and final steady state void fraction distributions as predicted by TRAC-P1A for vertical pipe ($\alpha_{initial} = 0.5$).
(BNL Neg. No. 2-546-80)

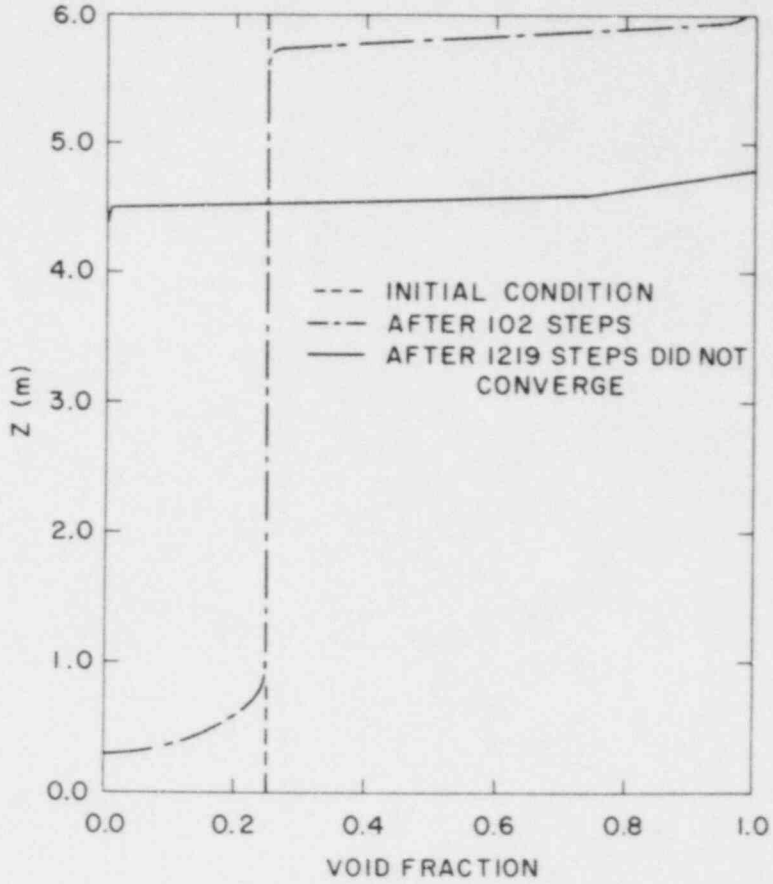

Figure 3.6 Initial and TRAC-P1A predicted void fraction distributions after 102 and 1219 steps for a vertical pipe ($\alpha_{initial} = 0.25$).
(BNL Neg. No. 2-545-80)

were performed at the exit level. Entrance void fraction and mixture velocity were equal to .1 and 5.0 m/sec, respectively.

The results obtained have shown that TRAC seems to have difficulty with the void fraction boundary condition when the two-phase flow enters the vessel. Jumps in average α-distribution in Z-direction took place (.1 at FILL, .01 at the first vessel level and .08 at the second one) whereas V_g distribution indicated that the gas mass equation was not fulfilled. The same thing should be pointed towards the liquid mass equation.

From this moment on FRIGG running was suspended until an understanding of what is going on with 3D two-phase hydrodynamics would be reached.

3.5 Various FLECHT Tests (L. Neymotin)

The FLECHT Tests results on reflooding heat transfer and hydraulic in a vessel are being studied and processed to prepare the input data deck.

3.6 Programming Considerations (Y. Sanborn)

TRAC-P1A updates given in July 1979 TRAC newsletter were incorporated into the TRAC-P1A code at BNL with identification TRAC-P1A/MOD1. The standard sample problems were run using TRAC-P1A/MOD1 and the results checked with those of LASL.

Spatial plotting capability of the BNL version of the associated plotting code, TRGRIT, was expanded to draw variable vs distance plots for one-dimensional components with the exception of TEE and Steam Generator. In the TRAC code, a call to the GRAF routine was added in the subroutine Steady, so that the graphic edit information is written on the graphic-edit file after the steady state is reached.

A BNL version of TRAC-P1A/MOD1, with more accurate surface tension calculation was made available.

3.7 Condensation Heat Transfer (P. Saha)

A literature survey of the condensation heat transfer has begun. The objective of this review is to recommend the most appropriate condensation heat transfer coefficients for the primary side of the steam generator when a two-phase steam-water mixture (with or without the noncondensible gases) flows through the primary tubes. This can be important in the small break analysis of PWR systems.

REFERENCES

JEANDEY, C. and BARRIERE, G., (1979), "Partie I : Etude Experimentale d'Ecoulements Eau-Air a Grande Vitesse," DTCE/STT/SETRE Note T.T. No. 599, Janvier 1979.

MAHAFFY, J. H., (1979), Private Communication, May 1979.

ROHATGI, U. S., (1980a), "Marviken Critical Flow Tests," in WRSRD Quarterly Progress Report, Reactor Safety Research Program, July - Sept. 1979, BNL-NUREG-51131, Jan. 1980.

ROHATGI, U. S., (1980b), "RPI Phase Separation Tests," in WRSRD Quarterly Progress Report, Reactor Safety Research Program, July - Sept. 1979, BNL-NUREG-51131, Jan. 1980.

SAHA, P., and FENG, Y., (1980), "Moby-Dick Nitrogen Water Experiments," in WRSRD Quarterly Progress Report, Reactor Safety Research Program, July - Sept. 1979, BNL-NUREG-51131, Jan. 1980.

II. METALLURGY AND MATERIALS EVALUATION

SUMMARY

The susceptibility of Inconel 600 to intergranular stress corrosion cracking (SCC) is being investigated in pure water, simulated primary water and environment with an all volatile treatment (AVT) typical of secondary side water in PWR steam generators.

U-bend tests have been completed in pure water at 365°C and 345°C, in primary water at 365°C and in AVT at 345°C. Failure times in all environments appear to be very similar at these test temperatures.

Constant stress tests are continuing with preliminary results indicating that failure times are inversely proportional to approximately the third power of the stress for one heat of material being tested.

Strain rate effects on crack velocity have been determined using the constant extension rate tests.

1. Stress Corrosion Cracking of PWR Steam Generator Tubing

(T.S. Bulischeck and D. van Rooyen)

The first draft of a report summarizing the program to date is near completion and will be sent to RSR for comments. A model for prediction of primary or secondary side SCC life of steam generator tubing under actual and varying steam generator service conditions is also included in this report.

Test Status

1.1 Constant Deflection Specimens

Results are detailed in Tables 1 and 1a. Circulating primary water tests at 365°C have been in progress for 23 weeks and will be terminated after the 24 week period. This test contained specimens fabricated from those heats of material which failed in pure water tests as well as some of the more recently received tubing materials. Commercial "thermally treated" (700°C for 20 hrs.) tubing as well as material removed from the process line prior to thermal treatment comprise this recently received group of materials. No failures have been found in any of the 4 heats of thermally treated material, however, 2 of the three heats of material which had identical processing history but without the 700°C - 20 hr. heat treatment failed during this time. Stress corrosion cracking was also found in 4 of the 5 heats of material which were susceptible to SCC in high temperature pure water environments. The failure times in primary water appear to be very similar to those obtained in pure water tests at this temperature. A primary water test at 345°C will be started near the end of January and this data will be used to complete the comparison between pure H_2O and primary H_2O environments.

The same heats of materials exposed to primary H_2O have been in an AVT environment at 345°C for 19 weeks. During this time, three of the five heats which cracked in pure water tests have failed. There doesn't appear to be any difference between failure in pure water and those in AVT at this time. Failure occurred in one heat of material exposed to an AVT environment in 1/3 of the time required in pure water, however, most of the other heats have failed in AVT at approximately the time necessary to produce SCC in pure water. None of the 700°C thermally treated material failed in this test and one of the new materials without thermal treatment failed. This test is scheduled to continue for several more weeks before starting a lower temperature study.

Pure water exposures at 325°C and 290°C are continuing with no new results to report at this time.

1.2 Constant Stress Tests

A dead weight loaded lever system which stresses three specimens simultaneously is now in operation. Specimens from one heat of material are loaded

with the three lever systems to different stress levels and failure times are recorded by micro-switch activated timers. The increased testing capacity of this system will be beneficial in providing essential data for crack initiation times as a function of stress and will permit the MTS system which is currently being used for this test to begin additional cyclic experiments.

The failure time dependence on stress level for specimens from Heat #4 (.01%C) is given in Figure 1. These specimens were stressed in 365°C pure water with the MTS system applying the controlled load. Examination of the fractured surface showed intergranular SCC approximately .045" into the .095" thick specimen. These preliminary results indicate that T_f is approximately proportional to σ^{-3} after normalizing the stress levels by subtracting the yield strength of the different specimens.

1.3 Constant Extension Rate Tests

These tests are continuing in two units with emphasis on establishing the crack velocities at or near operating conditions for several heats of material. The effect of strain rate is also being explored and current results indicate the crack velocity produced in a range of 10^{-6} sec^{-1} to 10^{-8} sec^{-1} is relatively linear with a slight increase in velocity as the rate is lowered.

Figure 2 indicates the crack velocity as a function of strain rate for two heats of material at two different temperatures. The average slope of these will be used to fulfill the requirement of determining strain rate effect, however, several more tests will be performed to determine the limits on these curves.

The third system is used as a sorting test to slowly strain 4 specimens in series and determine SCC susceptibility rather than crack velocities. Thermally treated materials are currently being tested in this system.

1.4 Capsule Tests

After 24 weeks exposure to 325°C primary water, capsules with an internal corrodant and carbon steel slug to provide deformation, have not shown any indications of SCC. Diametral deformation is approximately .019" after this period.

Table 1 Materials Experiencing IGSCC in U-bend Tests

Heat No.	Specimen Condition	Test Temp. (°C)	Environment	Specimens Failed Specimens Tested	Average Time to Failure (Weeks)	Exposure Time of Unfailed Specimens
2	As rec'd	365	H_2O	3/4	2	36
	Pickled		H_2O	2/2	2	-
	As rec'd	345	H_2O	2/2	14	-
	Pickled		H_2O	2/2	16	-
	As rec'd	325	H_2O	0/2	-	52
	Pickled		H_2O	0/2	-	52
	As rec'd	365	primary	2/2	4	-
	As rec'd	345	AVT	2/2	5	-
4	As rec'd	365	H_2O	2/2	11	-
	Pickled		H_2O	0/2	-	18
	As rec'd	345	H_2O	0/2	-	36
	Pickled		H_2O	2/2	10	-
	As rec'd	325	H_2O	1/2	51	52
	Pickled		H_2O	0/2	-	52
	As rec'd	365	primary	2/2	12	-
	As rec'd	345	AVT	2/2	7	-
5	As rec'd	365	H_2O	4/4	12	-
	Pickled		H_2O	1/4	9	30
	As rec'd	345	H_2O	2/2	16	-
	Pickled		H_2O	2/2	13	-
	As rec'd	325	H_2O	0/2	-	52
	Pickled		H_2O	1/2	29	52
	As rec'd	365	primary	0/2	-	23
	As rec'd	345	AVT	2/2	19	-

Table 1a Materials Experiencing IGSCC in U-bend Tests

Heat No.	Specimen Condition	Test Temp. (°C)	Environment	Specimens Failed Specimens Tested	Average Time to Failure (Weeks)	Exposure Time of Unfailed Specimens
10	As rec'd	365	H_2O	0/2	-	36
	Pickled		H_2O	2/2	2	-
	As rec'd	345	H_2O	0/2	-	36
	Pickled		H_2O	2/2	5	-
	As rec'd	325	H_2O	0/2	-	52
	Pickled		H_2O	0/2	-	52
	As rec'd	365	primary	2/2	21	-
	Pickled		primary	2/2	1	-
	As rec'd	345	AVT	0/2	-	12
	Pickled		AVT	2/2	8	-
11	As rec'd	365	H_2O	1/2	13	34
	Pickled		H_2O	2/2	4	-
	As rec'd	345	H_2O	0/2	-	36
	Pickled		H_2O	2/2	16	-
	As rec'd	325	H_2O	0/2	-	52
	Pickled		H_2O	0/2	-	52
	As rec'd	365	primary	1/2	22	23
	Pickled		primary	2/2	1	-
	As rec'd	345	AVT	0/2	-	20
	Pickled		AVT	2/2	11	-
17	As rec'd	365	primary	0/2	-	23
	Pickled		primary	2/2	14	-
	Pickled	345	AVT	1/2	17	18
18	As rec'd	365	primary	0/2	-	23
	Pickled		primary	1/1	17	-
	Pickled	345	AVT	2/2	9	-
20	As rec'd	365	primary	2/2	14	-
	Pickled		primary	1/2	5	18
	Pickled	345	AVT	0/2	-	18

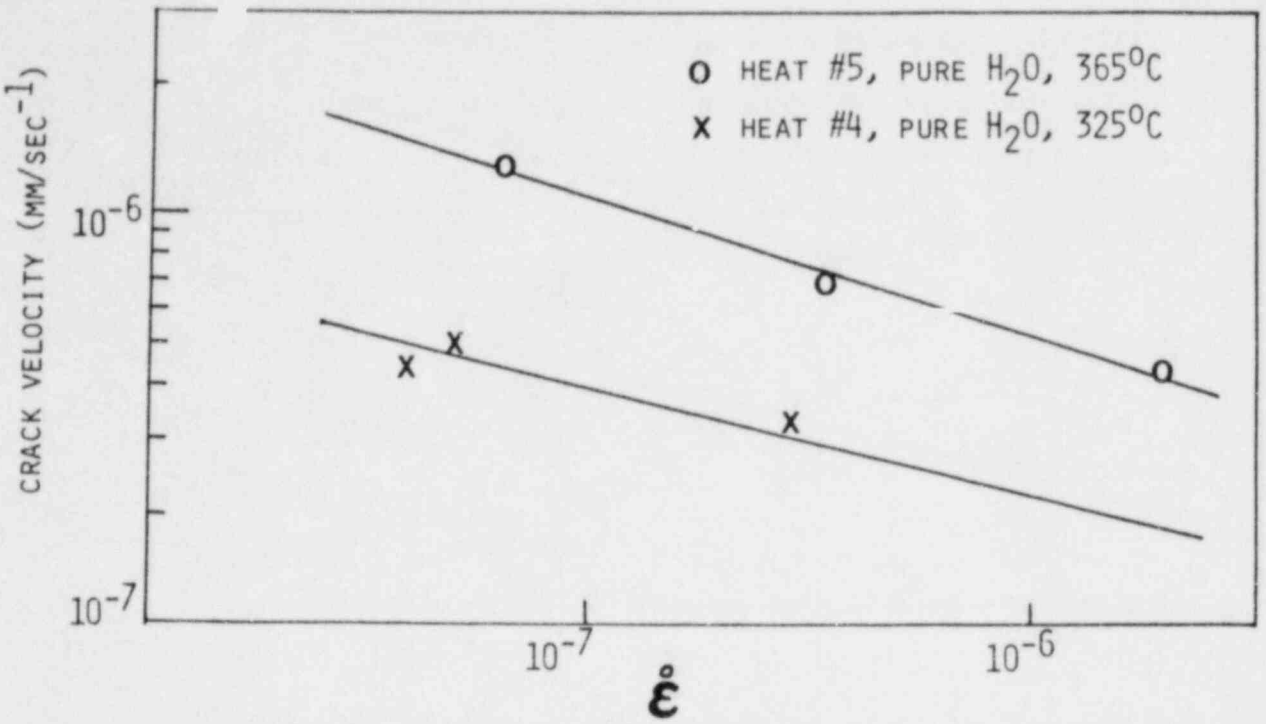

FIG. 1 EFFECT OF STRAIN RATE ON CRACK VELOCITY

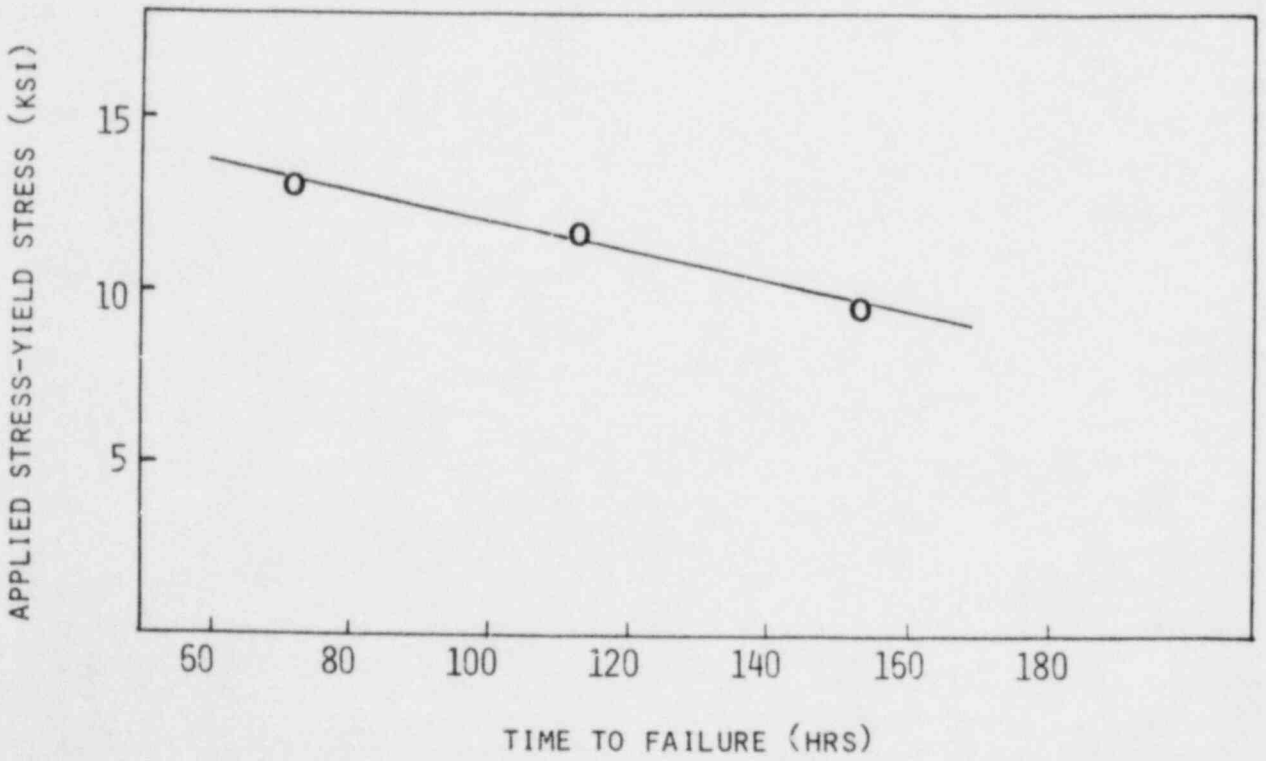

FIG. 2 PRELIMINARY CONSTANT STRESS TEST RESULTS WITH HEAT #4 IN D.I. H_2O @ 365°C